AD A113394

High-Resolution Radar Sea Scatter, Experimental Observations and Discriminants

JAMES P. HANSEN AND VINCENT F. CAVALERI

Target Characteristics Branch
Radar Division

March 5, 1982

DTIC
SELECTED
APR 9 1982
H

NAVAL RESEARCH LABORATORY
Washington, D.C.

82   04   09   046

REPORT DOCUMENTATION PAGE		READ INSTRUCTIONS BEFORE COMPLETING FORM
1. REPORT NUMBER NRL Report 8557	2. GOVT ACCESSION NO.	3. RECIPIENT'S CATALOG NUMBER
4. TITLE (and Subtitle) HIGH-RESOLUTION RADAR SEA SCATTER, EXPERIMENTAL OBSERVATIONS AND DISCRIMINANTS		5. TYPE OF REPORT & PERIOD COVERED Interim report on a continuing NRL problem
		6. PERFORMING ORG. REPORT NUMBER
7. AUTHOR(s) James P. Hansen and Vincent F. Cavaleri		8. CONTRACT OR GRANT NUMBER(s)
9. PERFORMING ORGANIZATION NAME AND ADDRESS Naval Research Laboratory Washington, DC 20375		10. PROGRAM ELEMENT, PROJECT, TASK AREA & WORK UNIT NUMBERS Program Element 62712N; Project No. SF12141491; NRL Prob. 53-0603-00
11. CONTROLLING OFFICE NAME AND ADDRESS Naval Sea Systems Command Washington, DC 20362		12. REPORT DATE March 5, 1982
		13. NUMBER OF PAGES 52
14. MONITORING AGENCY NAME & ADDRESS(if different from Controlling Office)		15. SECURITY CLASS. (of this report) UNCLASSIFIED
		15a. DECLASSIFICATION/DOWNGRADING SCHEDULE

16. DISTRIBUTION STATEMENT (of this Report)

Approved for public release; distribution unlimited.

17. DISTRIBUTION STATEMENT (of the abstract entered in Block 20, if different from Report)

18. SUPPLEMENTARY NOTES

19. KEY WORDS (Continue on reverse side if necessary and identify by block number)

High-resolution radar   Low incidence
Radar   Target detection
Sea scatter
Sea spikes

20. ABSTRACT (Continue on reverse side if necessary and identify by block number)

An experimental study was made of the characteristics of high-resolution, low-incidence-angle, radar sea scatter. The experiment utilized measurements made with several radar systems with varying pulsewidth, frequency, and polarization while the radar-illuminated sea surface was observed optically.

Measurements were performed at both shallow-water and deep-water sites, and they revealed that all high-resolution, X-band radar, sea return is heavily amplitude modulated pulse-to-pulse,

(Continued)

DD FORM 1473 EDITION OF 1 NOV 65 IS OBSOLETE
1 JAN 73
S/N 0102-014-6601

20. ABSTRACT (Continued)

with modulation frequencies significantly higher than those expected from rigid targets. Moreover, under many conditions of wind and sea the backscatter in individual range-resolution cells was found to be characterized by significant periods of extremely low level return interspaced between relatively high level spikes. High-level returns were often associated with turbulent breaking water, as indicated by whitecaps. Some marked distinguishing features were also noted in the spatial and time-varying characteristics of the high-resolution sea scatter as a function of radar polarization. For upwind conditions and vertical polarization, it was observed that backscatter was consistently evident from many portions of the nonshadowed sea surface, while horizontal polarization produced sporadic returns, often with a "burstlike" character. The distribution and level of the data taken with vertical polarization generally agreed with those taken at lower resolution by other researchers, while the data taken with horizontal polarization tended to be more nonexponential in character.

The experimental data have contributed to an initial theoretical model of sea-scatter phenomena and were also used to demonstrate a clutter-rejection discriminant based on the relative pulse-to-pulse amplitude-modulation characteristics of sea clutter and rigid targets.

CONTENTS

HIGH-RESOLUTION RADAR SEA SCATTER, EXPERIMENTAL OBSERVATIONS AND DISCRIMINANTS

INTRODUCTION

This report describes work done in connection with small-target detection techniques. The primary objective was to develop concepts for improved radar-detection performance against a sea background.

High-resolution radar detection of small objects lying low in the water is often made difficult by the presence of targetlike clutter echoes from the sea surface. (Figure 1 shows examples of typical disturbed sea surfaces. Note the various facets and contours which are presented to an observing radar system.) Techniques which discriminate against sea clutter yet preserve target signals could be applied to a variety of radar problems, ranging from collision avoidance by high-speed ships to periscope detection.

Two goals of this experimental study were to characterize the radar-echoing qualities of the sea surface and of small floating targets and to devise and demonstrate the feasibility of hardware approaches to satisfy the specialized radar requirements. The experimental approach toward these goals consisted of measuring the echoing characteristics of sea clutter and small targets, as functions of the controllable parameters of pulsewidth, frequency, and polarization, while optically observing physical changes in the scattering surface. Sea-return measurements were carried out with several X-band systems at both shallow-water and deep-water sites and over a varied range of sea and wind conditions. These quantitative data have contributed to an initial theoretical model of sea-scatter phenomena [1-3] and have also been used to demonstrate a new sea-clutter discriminant based on differences in the pulse-to-pulse amplitude modulation characteristics of sea return and of rigid targets.

During the experimental program it was found that high-resolution sea scatter was dependent on many dynamic conditions of wind and sea. The physical environment is so changeable that long-term data averages can tend to obscure some of the more interesting features. This report has therefore been organized around specific samples in an attempt to present to the reader some of the varied character seen in actual high-resolution radar observations of the sea surface.

EXPERIMENTAL MEASUREMENT SYSTEMS

Several systems were developed and utilized to study the characteristics of high-resolution radar sea return. Block diagrams of the measurement systems and data-recording complexes are shown in Figs. 2 to 4.

The dual-frequency, single-range-cell system shown in Fig. 2(a) used two continuous-wave (cw) signal generators as carrier sources (nominally tuned to 8.6 GHz and 9.2 GHz). The outputs of these two generators were added in a hybrid circuit and amplified; the hybrid signal then excited the input of a diode switch for pulse shaping. The minimum usable pulse length was 20 ns, and the maximum pulse length was limited by the pulse repetition period of the timing generator, which was variable from 0.02 to 1 ms. The antenna was a parabolic reflector, either 1 or 2.67 m in diameter, with orthogonal, linearly polarized feeds separately connected to a polarization switch.
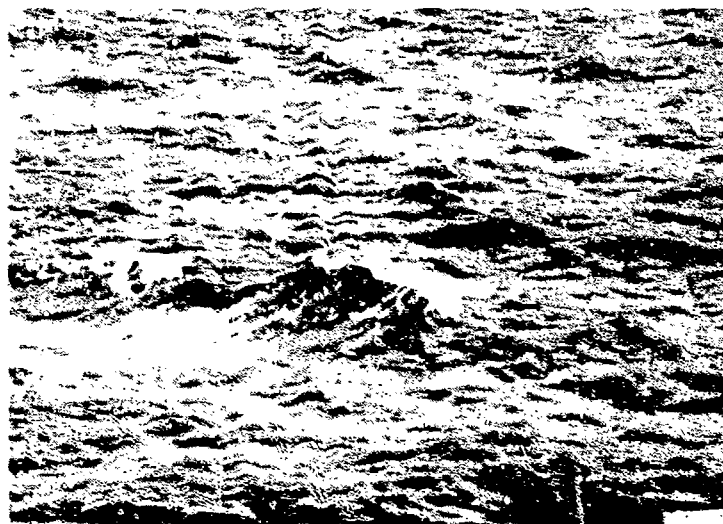
1

(a)

(b)

Fig. 1 — A disturbed sea surface (a) sea state 2, (b) sea state 4

Radar echoes that entered the antenna passed through the polarization switch and entered the radar receiver through the circulator and a diode switch that was closed by a receiver gate pulse from the timing generator. The output from this switch passed through a calibrated variable attenuator and was amplified by a low-noise traveling-wave tube (TWT) chain. The output of the TWT chain entered port A of a four-port circulator and coupled to a 200-MHz-wide bandpass filter tuned to 8.6 GHz and attached to port B of the circulator. The 8.6-GHz signal passed through this filter, and the 9.2-GHz signal reflected back into port B of the circulator. The 9.2-GHz signal exited from port C of the circulator and passed through another bandpass filter tuned to 9.2 GHz. The outputs of these two filters were rectified in separate detectors and amplified in separate wideband video amplifiers. These amplifier outputs were displayed as real-time video on a two-channel oscilloscope and were also used as inputs to two range-gated sample-and-hold circuits. The gated stretched outputs of the sample-and-hold circuits were displayed as time functions on a two-channel oscilloscope and were also recorded on a two-channel magnetic tape recorder. This presentation showed the amplitude-time history of the power received from a single range cell.

Some initial measurements were also carried out with a dual-frequency system transmitting X-band and S-band signals (9.2 and 3.0 GHz). The general layout of the system was similar to the dual X-band system, except that two TWT chains were used with separate parabolic antennas (1 m for X-band and 1.6 m for S-band).

Figure 2(b) is a schematic of the data-recording complex for the dual-frequency systems. A television camera with a zoom lens was mounted on the radar antenna with its field of view centered on the radar field of view. Two other television cameras were used to record the real-time video and the range-gated time functions displayed on two-channel oscilloscopes. Split-screen techniques were used to record the output of all three television cameras on the same television recorder. This ensured time synchronization of the radar data and the optical picture of the sea surface that produced the radar echoes.

Figure 2(c) shows the typical TV video display produced by this data-recording system. The right-hand section of this picture is the view from the boresight camera. The inset at the bottom left is the real-time video and the range gate. The lower trace is 8.6 (or 3.0) GHz, the middle trace is 9.2 GHz, and the upper trace is the approximate range-gate position. The sweep speed for the real-time video was 50 ns/cm, or 500 ns per sweep. The inset at the top left is the gated stretched video, with 9.2-GHz top trace and 8.6-GHz bottom trace. The sweep speed of these traces was 20 ms/cm (0.2 s per sweep). The circular dark spot on the boresight picture is the region filled by the radar beam at ranges long enough to minimize the parallax between the TV camera and the antenna. The dotted lines in this dark spot are the region covered by the 20-ns range gate when the beam strikes the water at a 4.6° grazing angle.

Figure 3 is a block diagram of the single-frequency, contiguous-range-cell measurement system. This system utilized a pulsed-magnetron signal source (centered at 9.3 GHz) as its basic transmitter. Diode switches were used to trim the nominal 300-ns transmit pulse down to 40 ns. The maximum repetition rate was 2.5 kHz. The real-time video for this system was fed into eight paralleled sample-hold circuits, which were sequentially gated every 40 ns over a time span of 320 ns. This time period provided a contiguous-range-cell coverage of approximately 50 m. The first four gated and stretched outputs were displayed as time functions on a four-channel oscilloscope. Seven of the outputs plus a time code were also recorded on an eight-channel magnetic tape recorder.

In the single-frequency system an additional TV video input was added to provide a synthetic range display of the pulse-to-pulse received-power levels of the eight contiguous range cells and also to record visually a time code for synchronization with the audio tape data.
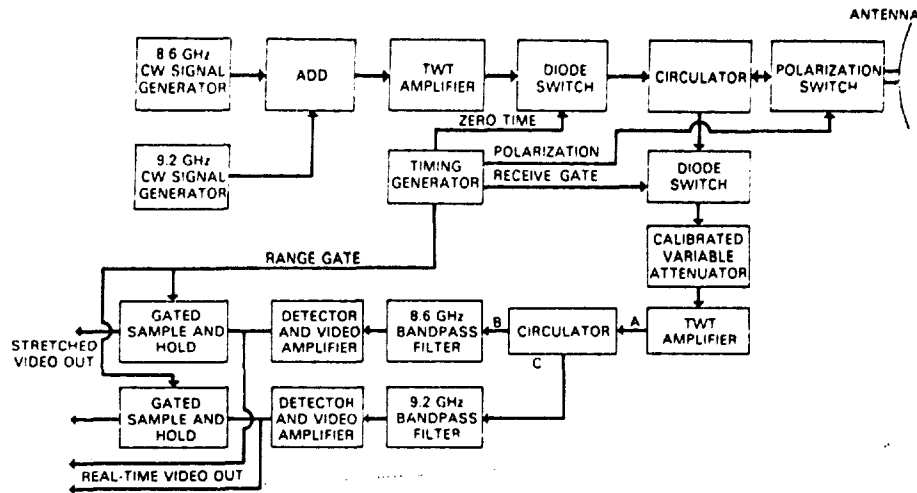
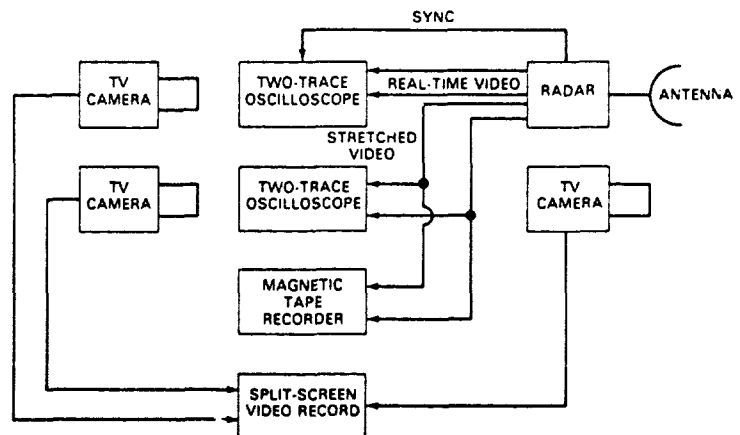Fig. 2(a) — The dual-frequency, single-range-cell measurement system

Fig. 2(b) — The dual-frequency, single-range-cell
data-recording complex

SEA-CLUTTER DATA FORMAT
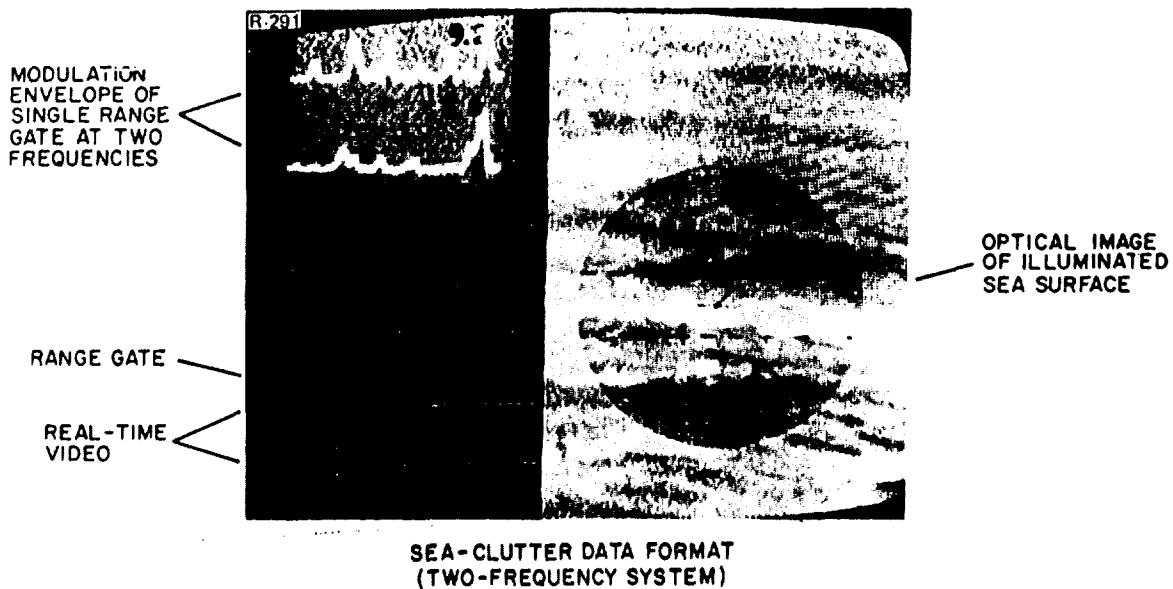(TWO-FREQUENCY SYSTEM)

Fig. 2(c) — The TV video display for the dual-frequency, single-range-cell measurement system
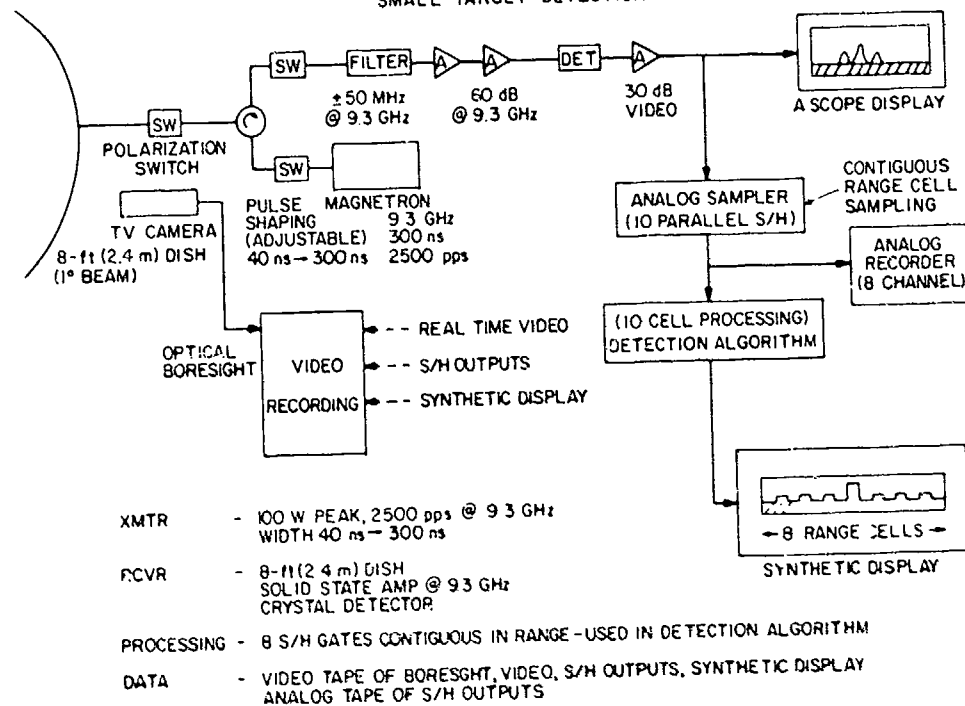
4

SMALL TARGET DETECTION RADAR

Fig 3 — The single-frequency, contiguous-range-cell
measurement system

Figure 4 shows the TV video display produced with this recording complex. The upper right-hand section of the picture is the view from the boresight camera. The inset at the bottom right shows the real-time video (top trace) and a pulse representing the coverage of the eight contiguous range gates (bottom trace). The video inset at the top left shows the gated stretched return signals for the first four range cells. Sweep speed for the real-time video was nominally 200 ns per division. Sweep speed for the stretched video was 20 ns per small division. The inset in the lower left shows the real-time video levels being received by the eight contiguous range cells, displayed in a synthetic eight-cell contiguous range format, and also the time code.
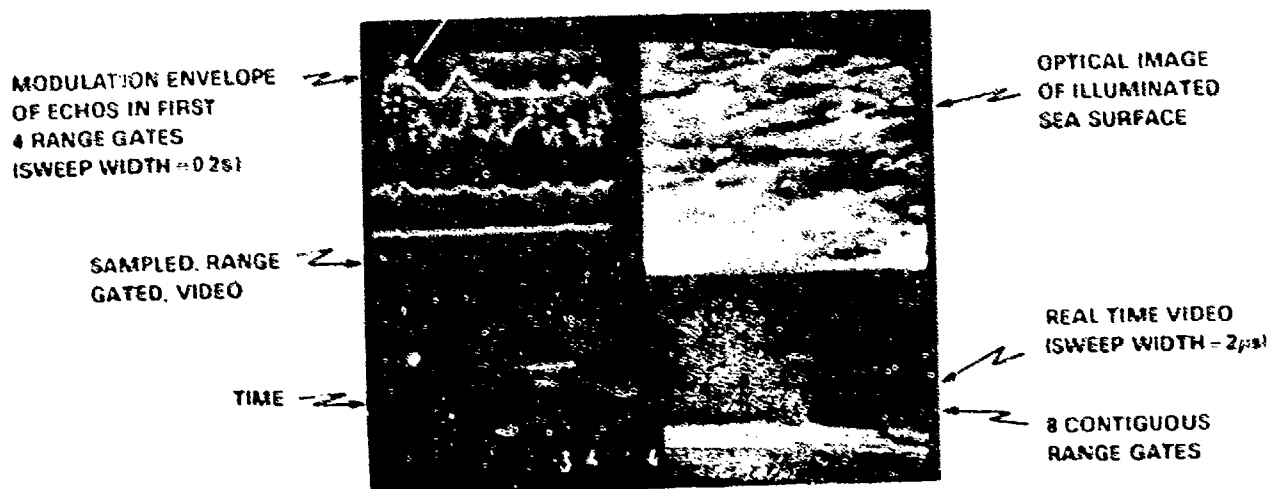
Fig 4 — The TV video display for the single-frequency
contiguous range-cell measurement system

CALIBRATION

The systems were calibrated and boresighted using corner reflectors (or spheres) with known equivalent scattering cross sections. Variable attenuators at the input to the receiver were adjusted so that both the real-time video and the gated stretched video were at the upper end of the linear range of the system. Calibration was made in the far field at the two shore sites (Chesapeake Bay, Maryland, and Boca Raton, Florida) and in the near field at the platform site (Stage I, Panama City, Florida). Figures 5 through 7 show pictures of the transmit-receive antennas and calibration setups for the various measurement systems.
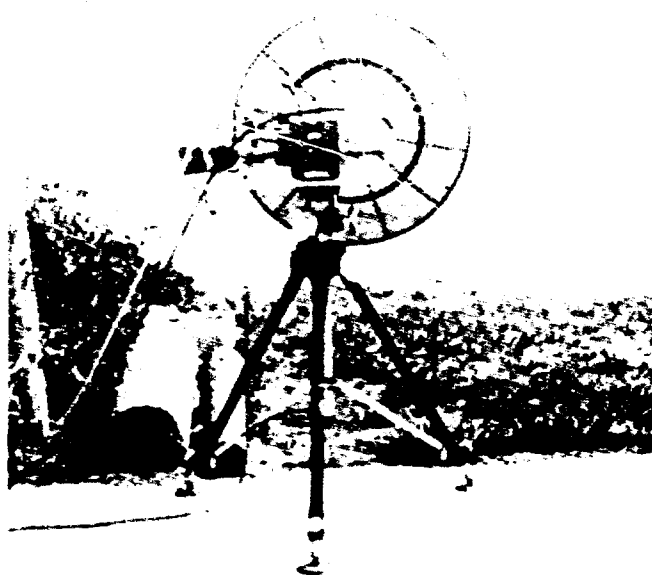
Fig. 5(a) — Measurement site, shallow-water data, Chesapeake Bay, Md., showing dual-frequency X-band system antenna
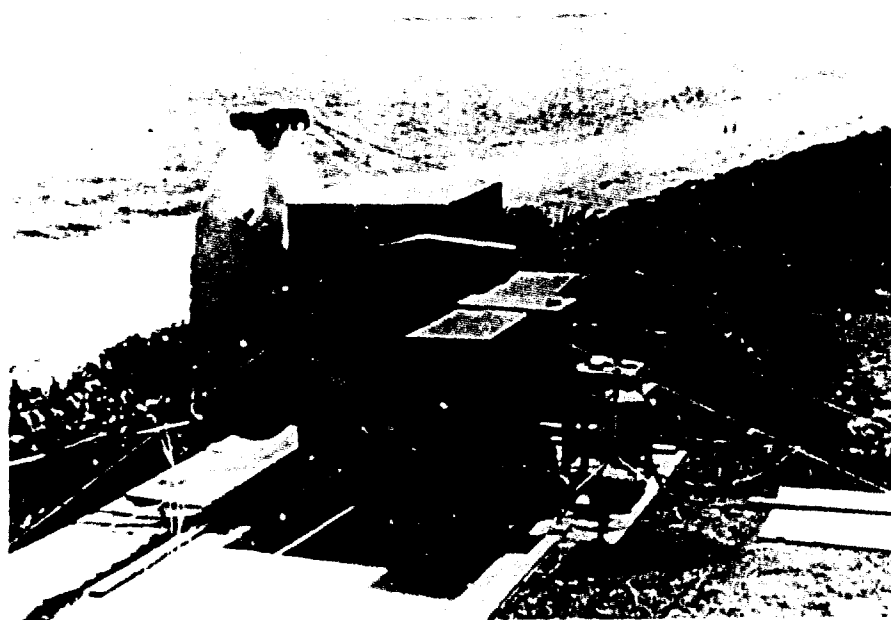
Fig. 5(b) — Measurement site, deep-water data, Boca Raton, Fla., showing dual-frequency X-band system antenna

6
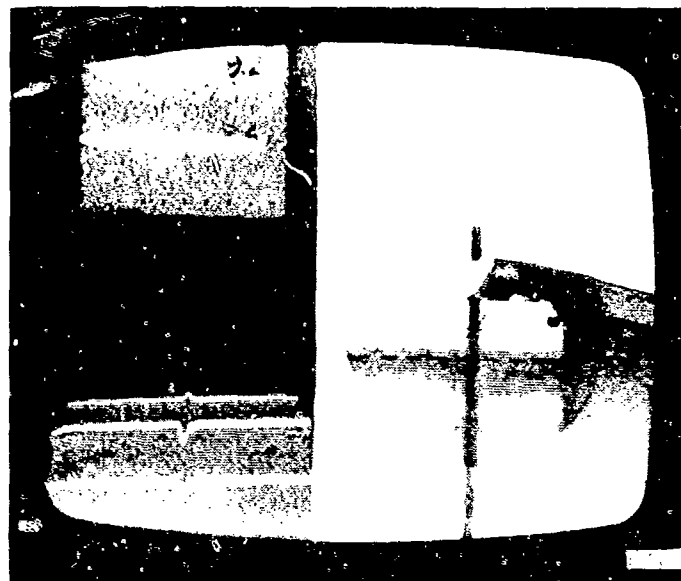
Fig. 5(c) — Calibration setup (corner reflector), dual-frequency
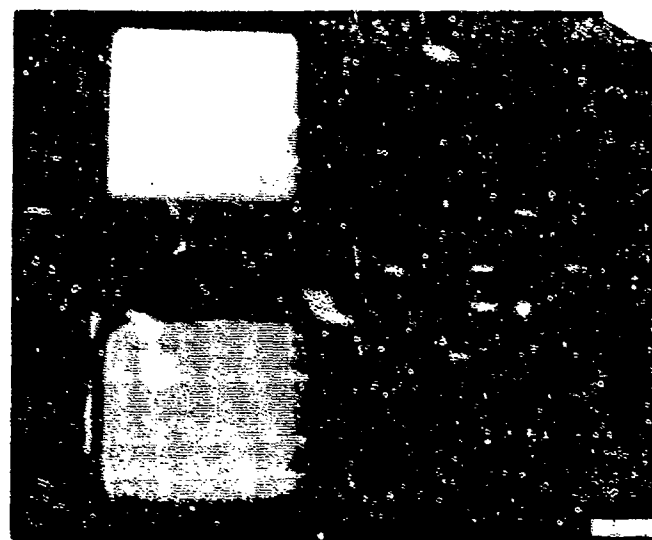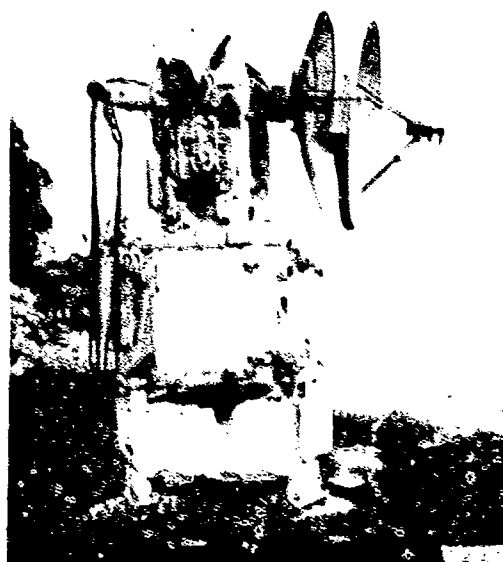X-band system, Chesapeake Bay, Md.

Fig. 6 — Antenna (a) and calibration setup (sphere) (b), S- and X-band system, Chesapeake Bay, Md.

(a)

(b)

Fig. 7 — Antennas (a) and calibration setup (center reflector) (b) single-frequency contiguous-band (full) system Stage I Program Cycle IIb

EXPERIMENTAL OBSERVATIONS

Shallow-Water Data (2-m Depth)

The first measurements of sea return were made at the Chesapeake Bay site [see Fig. 5(a)] with the dual-frequency, single-range-cell system and with a 1-m-diameter radar antenna, 4 m above the mean water level. The radar beamwidth with this antenna was 2.6°, and the center of the beam impinged on the water at a distance of 50 m. These values yielded a 2-m cross-range resolution cell at the center of the beam and a grazing angle of 4.6°. The radar pulse length and range gate were 20-ns long, yielding a range resolution of 3.33 m.

Figures 8(a) and 8(b) typify data obtained with vertical and horizontal polarization and with 1- to 1.3-m waves. The individual pictures were taken sequentially with approximately 0.3 s between pictures. This time interval corresponded to the time between sweeps of the oscilloscope which shows the gated stretched video. All data were taken in a generally upwind direction.

These dual-frequency, single-range-cell, shallow-water measurements allowed close correlation between the physical changes in the radar-illuminated sea surface and the received backscatter. The following conclusions were reached from these data [1,2]:

●The backscatter was heavily amplitude modulated with relatively high frequencies, of the order of 20 to 100 Hz. (See Figs. 9(a) and 9(b) for examples of pulse-to-pulse stretched data under two different surface conditions.)

●Large backscatter amplitudes were associated with the turbulent breaking action of the water (whitecaps) but not with the residual foam left after the breaking action. Slightly disturbed surfaces (by wind or rain) also produced a characteristic low-level but spikelike backscatter, as in Fig. 9(b). Figures 10 and 11 show examples of backscatter from wind- and rain-disturbed surfaces, as seen on an A-scope.

● The short-term fluctuations between the the envelopes of the spikelike returns from two transmitted frequencies suggested a multipath effect involving the breaking water and its image in the crest. Simultaneous observation of an optical reflection of the whitecap in the crest supported this conclusion.

● With vertical polarization and normal wave-crest alignments to the radar, high-amplitude spike returns would sometimes occur slightly prior to the visually observed formation of whitecaps.

● Observation of the sea surface with a dual X- and S-band system suggested that the characteristic amplitude modulation tends to scale down in frequency with increased transmitted wavelength. Figure 12 shows examples of these data. Note that the modulation frequencies for the X-band return (top trace) are generally a factor of two to three higher than the S-band return (second trace) for the same radar-illuminated surface.

Deep-Water Data (12.3-m Depth)

Sea-return measurements were also made at Boca Raton, Florida, in deep water with the dual-frequency, single-range-cell system [see Fig. 5(b)]. In these measurements, the 2.67-m-diameter (1° beamwidth) antenna was employed. The antenna was mounted on top of a building 13 m above mean sea level, and the center of the beam intercepted the water at a distance of 530 m. This produced a grazing angle of about 1.4°. The boresight-camera field of view was narrowed to permit it to cover the radar beam in azimuth (1°) on the split-screen display, and it provided a 2° vertical field of view.
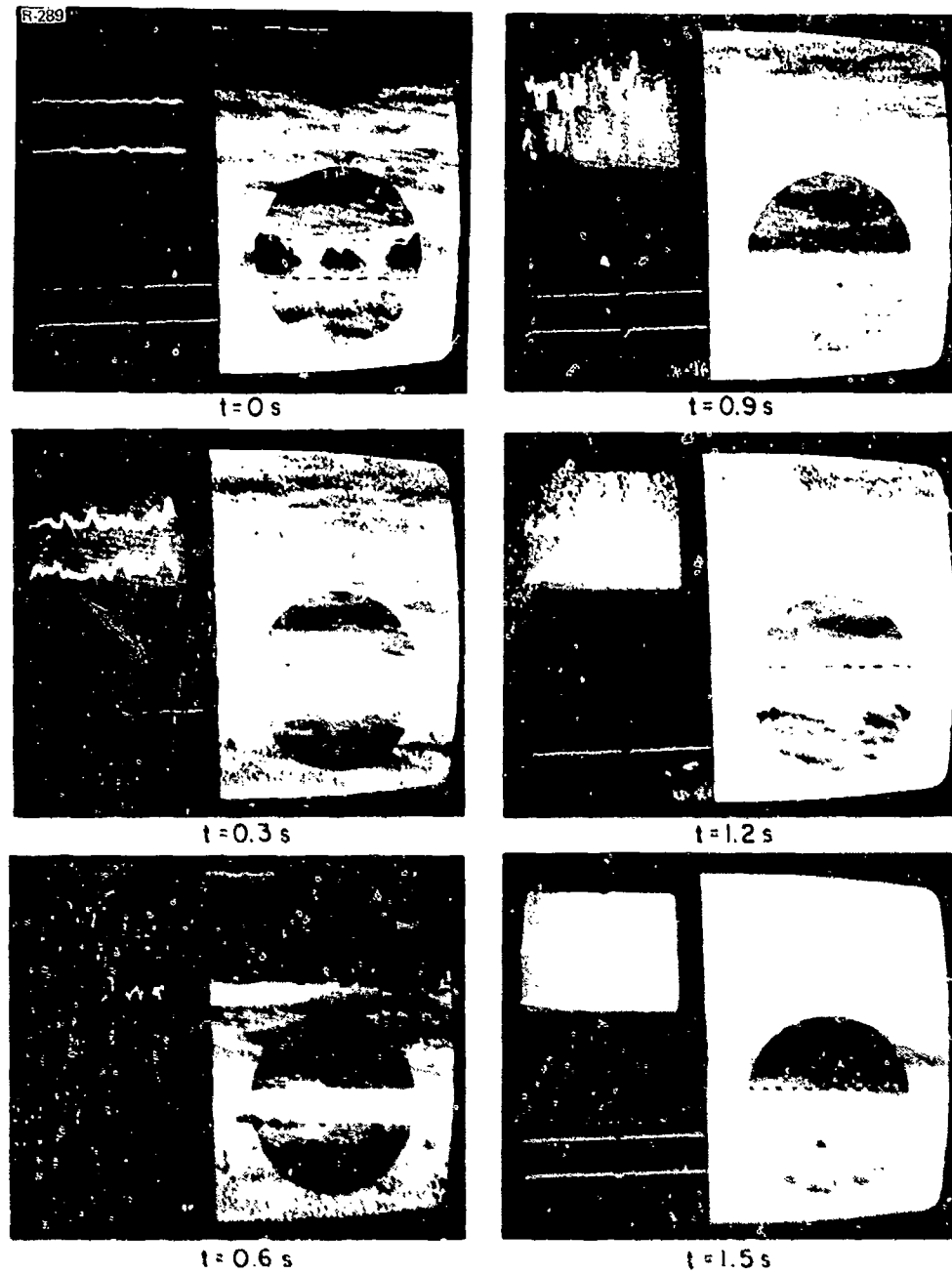
Fig 8(a) — Typical TV video data, sequential photos, shallow water, dual-frequency X-band system vertical polarization
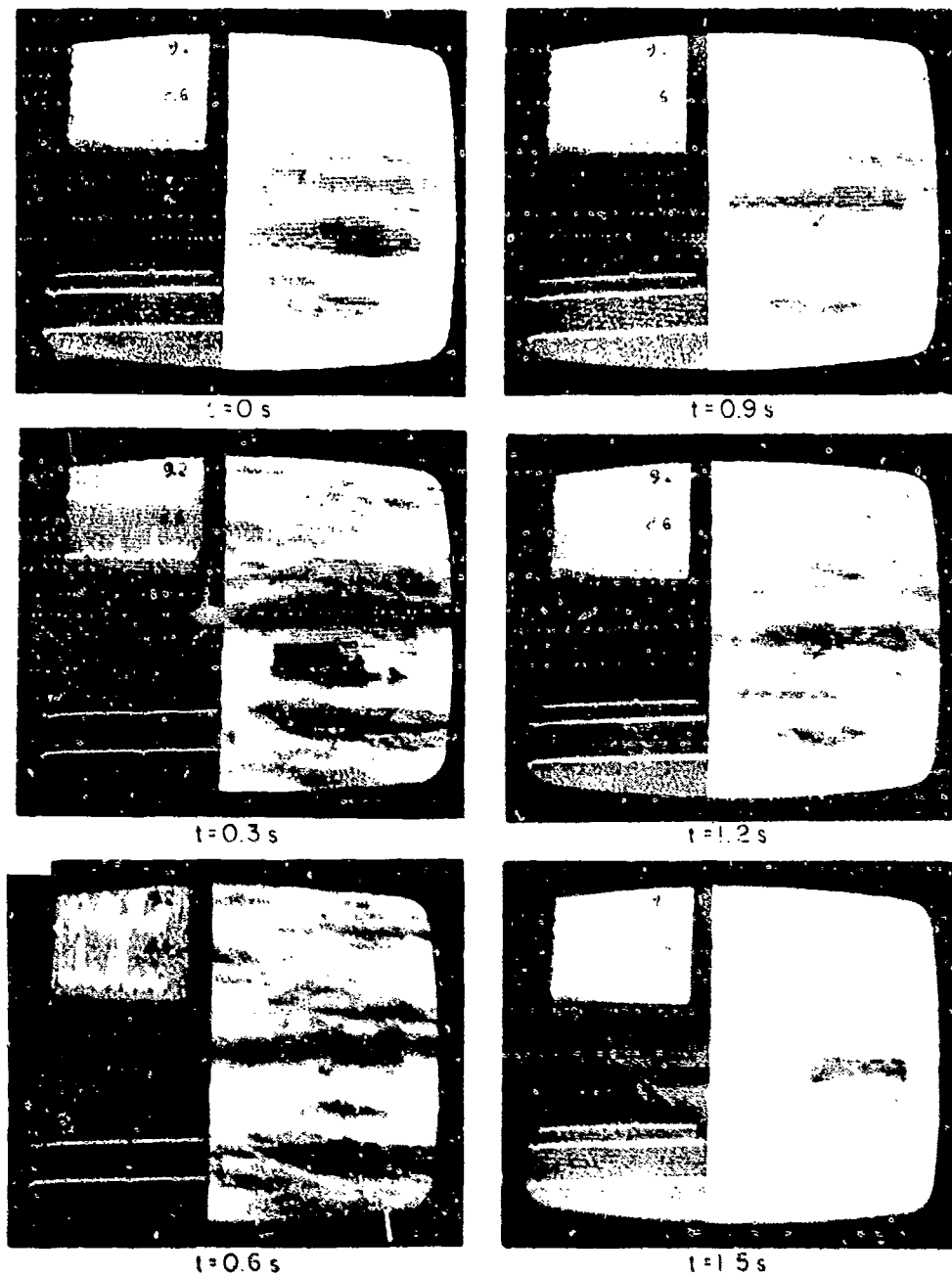
Fig. 8(b) — Typical IX video data, sequential photos, shallow water, dual-frequency X-band system horizontal polarization
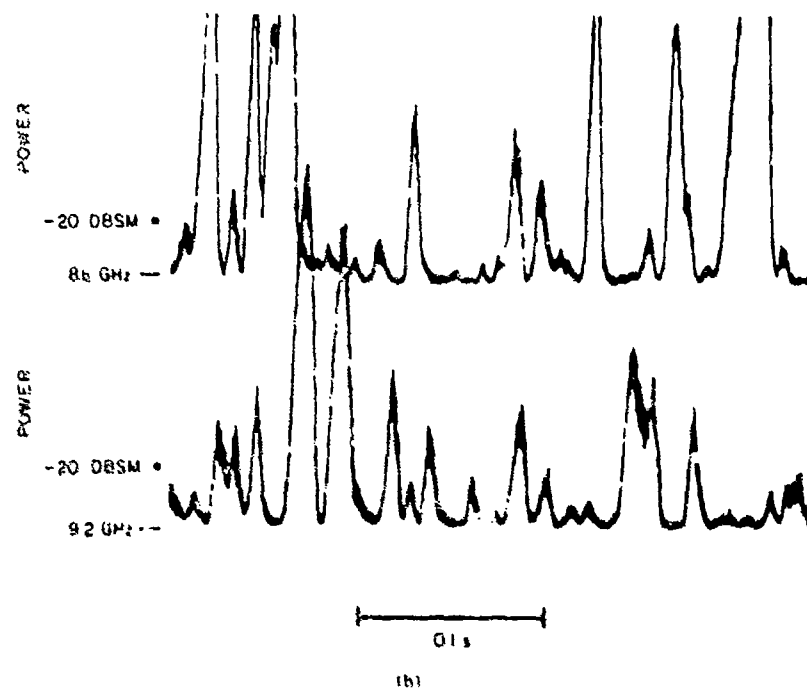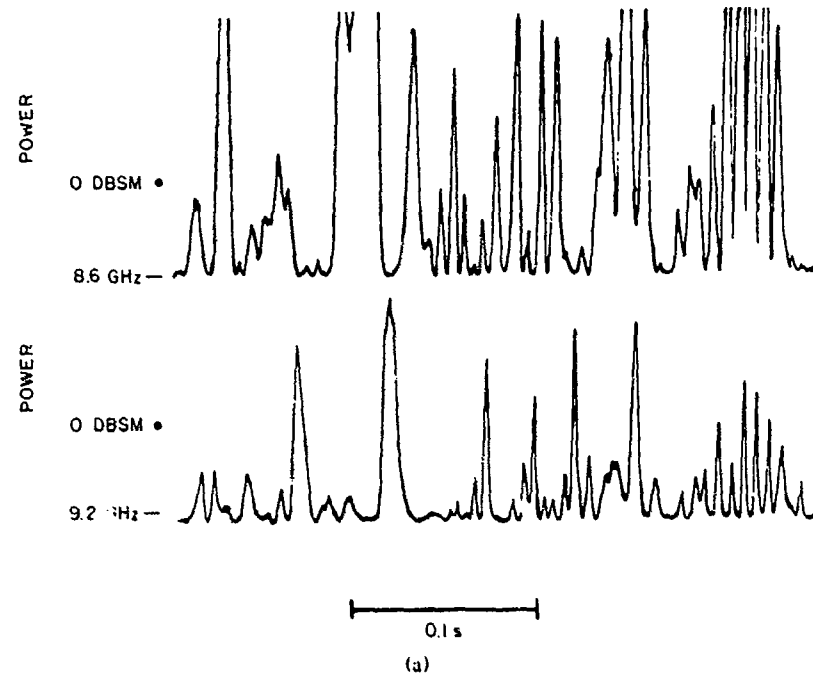
POWER

O DBSM •

8.6 GHz —

POWER

O DBSM •

9.2 GHz —

0.1 s

(a)

POWER

−20 DBSM •

8.6 GHz —

POWER

−20 DBSM •

9.2 GHz —

0.1 s

(b)

Fig. 9 — Pulse-to-pulse amplitude of scatter, vertical polarization: (a) from breaking wave (whitecap), (b) from relatively undisturbed sea (no whitecaps)

(a)   (b)
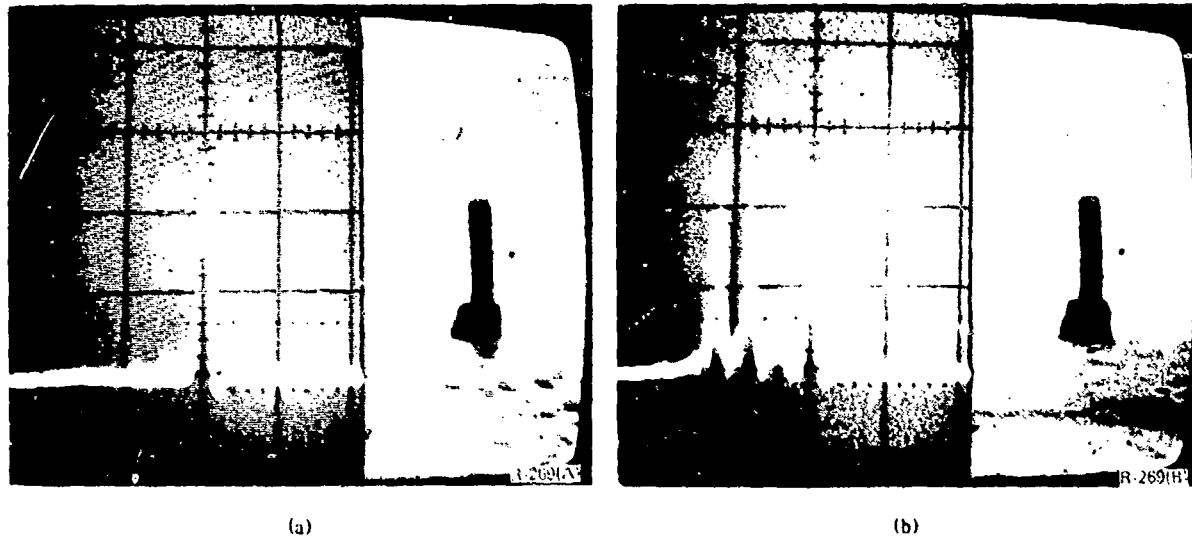
Fig. 10 — A-scope photos of high-resolution scatter from a wind-disturbed sea surface:
(a) return from wooden post at edge of illuminated sector;
(b) scatter returns from the wind-distributed sea surface surrounding the post

(a)   (b)
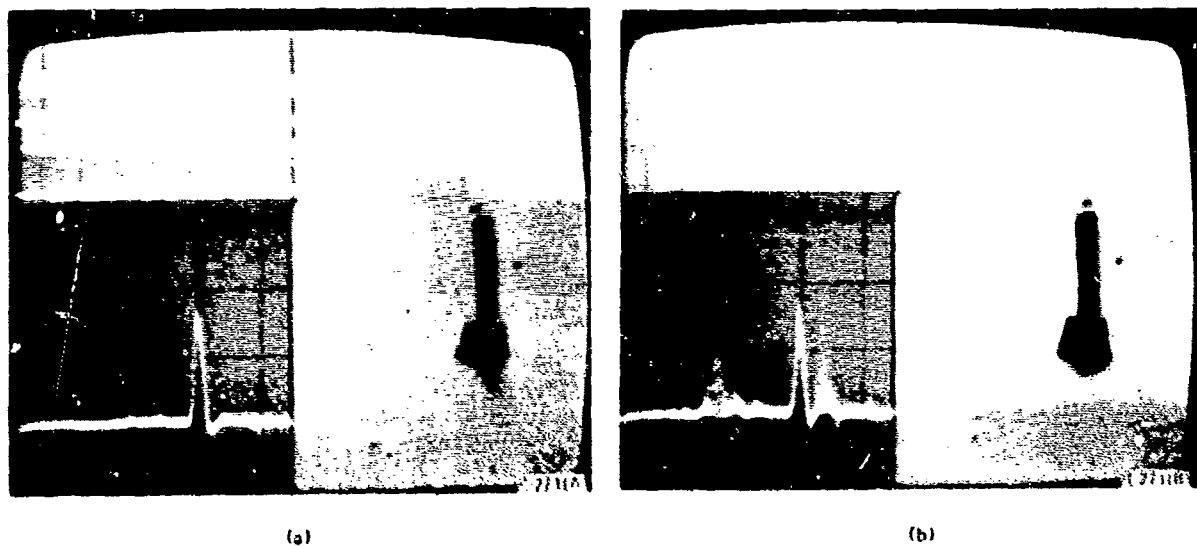
Fig. 11 — A-scope photos of high-resolution scatter from a calm, rain-disturbed sea surface:
(a) return from wooden post just prior to a rain squall;
(b) scatter returns from the rain-disturbed sea surface surrounding the post
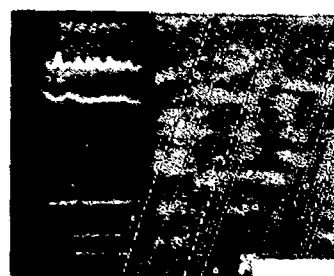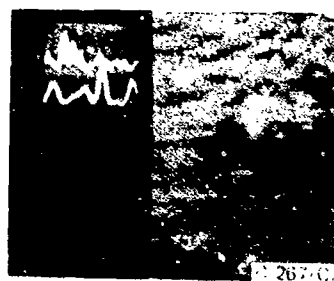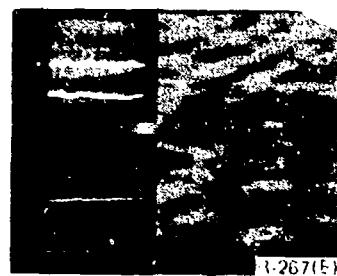
Fig. 12 — Typical TV video data, vertical polarization, shallow water, dual-frequency X- and S-band system. Top trace in each photo is X-band return, second trace is S-band return.

The 530-m range and 1° beamwidth produced an azimuth resolution of about 9 m, and the 40-ns pulse yielded a range resolution of 6.2 m (56 m² cell area).

Figure 13 typifies the TV video data obtained at this site in approximately sea states 1 and 3 (sea state 3, relative 30-dB attenuation). These single-range-cell, dual-frequency data were taken with several transmitted-pulse widths for both horizontal and vertical polarization. The data reconfirmed some of the initial shallow-water test results and also demonstrated a backscatter dependence on transmitted-pulse width and polarization [3]:

1. The temporal characteristics of radar backscatter from the sea strongly depend on pulse width for surface resolutions less than about 20 m. Low-resolution backscatter appears continuously noise-like, but as resolution is increased, the backscatter is punctuated by substantially quieter periods. This results in a noticeably spikelike characteristic on an amplitude-time record. The observations confirmed that large backscatter is often associated with whitecaps. However, even the quieter periods disclosed spikelike returns, although they were several orders of magnitude lower in power. The stretched, single-cell data, as displayed in the chart recordings shown in Figs. 14 and 15, illustrate the changes in the frequency of occurrence of sea return as a function of transmitted-pulse width for both calm and rough-sea conditions (RCS = radar cross section). Figures 16 and 17 show examples of video returns on an A-scope display for 1/30-s exposure times at various transmitted-pulse widths.
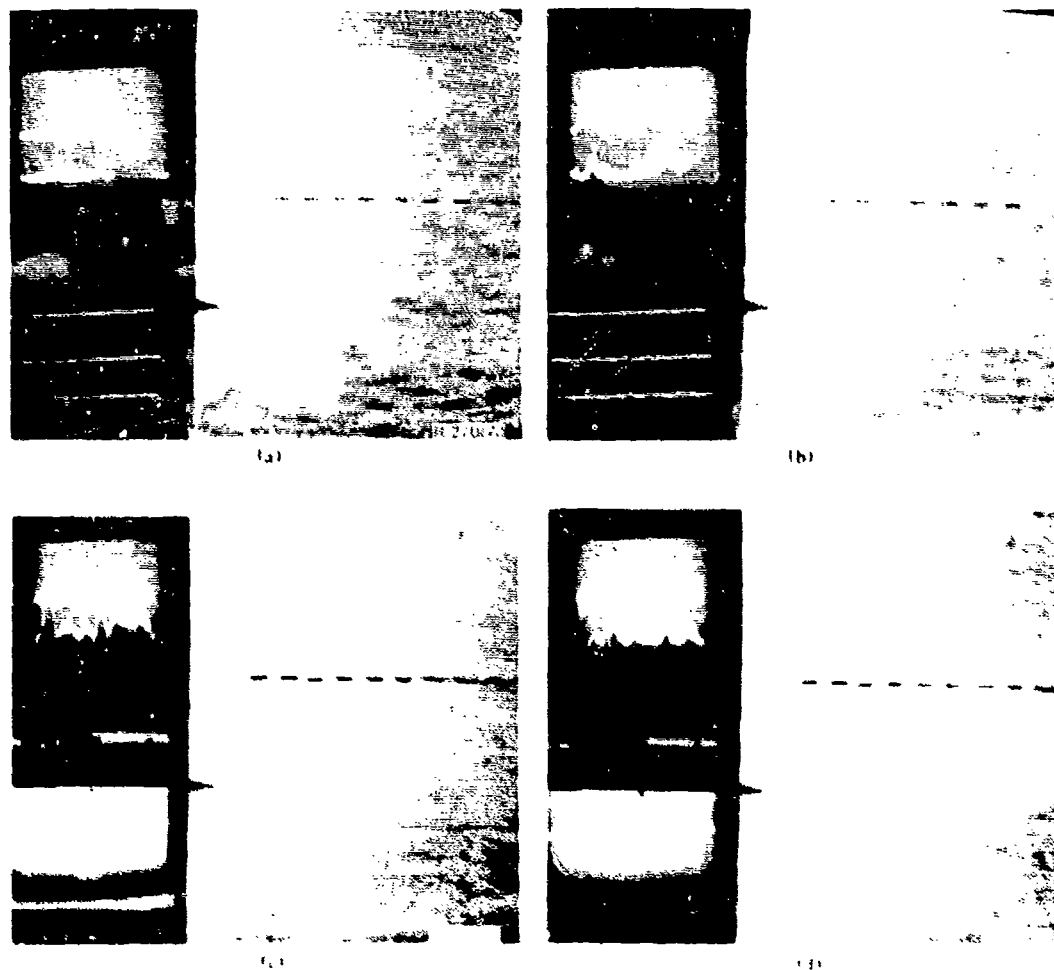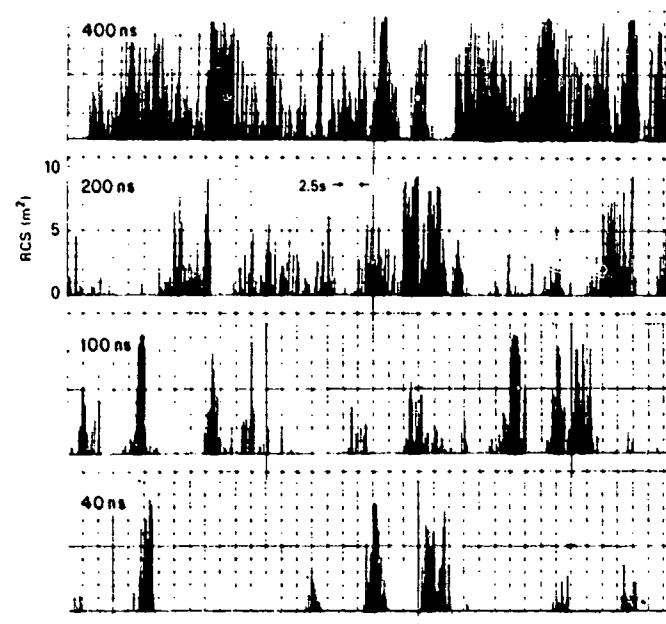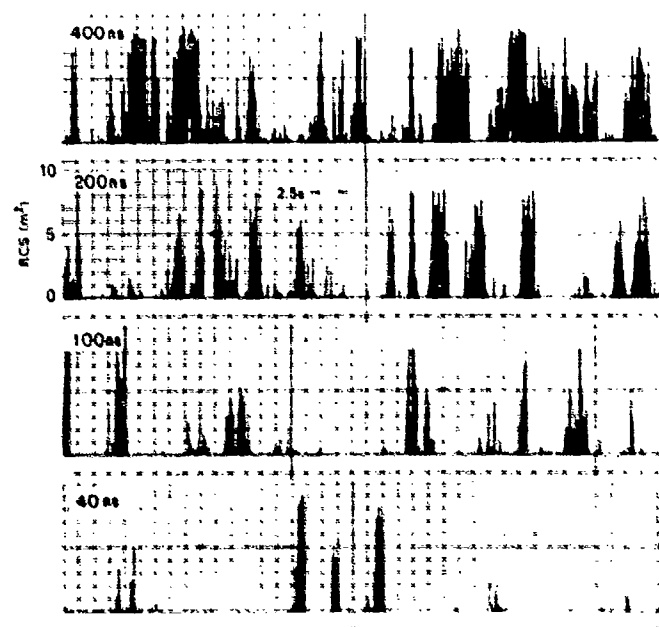

(a) (b) (c) (d)

Fig. 13 — Typical TV video data, deep water, dual-frequency X-band system. (a) vertical polarization, sea state 1, (b) horizontal polarization, sea state 1, (c) vertical polarization, sea state 3, (d) horizontal polarization, sea state 3
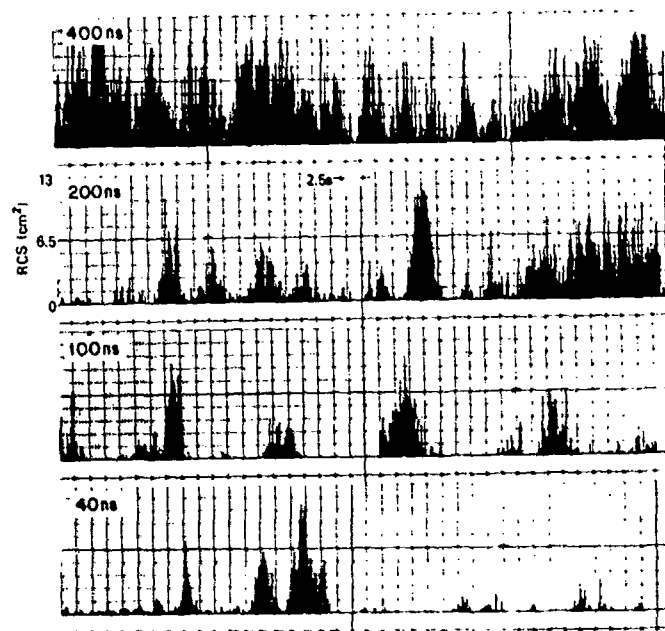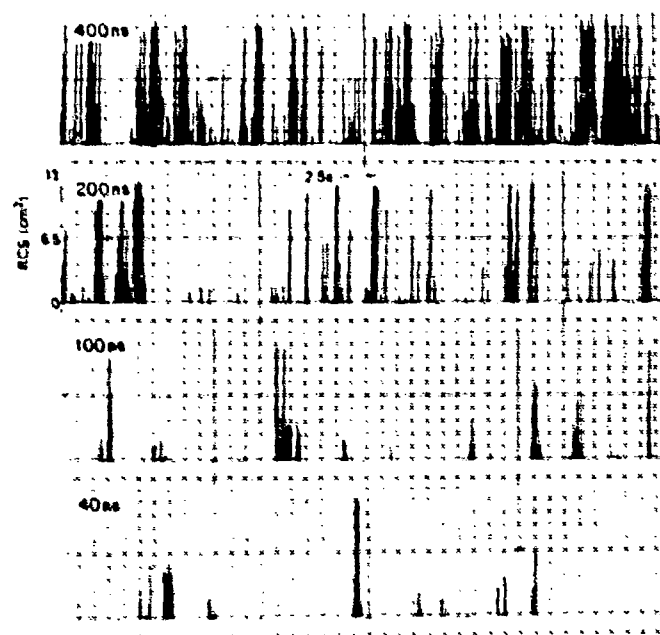
Fig 14 — Pulse-to-pulse amplitude of scatter for sea state 3, with pulse widths from 400 to 40 ns (scales: 1 m² per div and 2.5 s per div.) (a) vertical polarization, (b) horizontal polarization

(a)

(b)

Fig. 15 — Pulse-to-pulse amplitude of scatter for sea state 1, with pulse widths from 400 to 40 ns (scales: 1.3 cm² per div. and 2.5 s per div.) (a) vertical polarization, (b) horizontal polarization
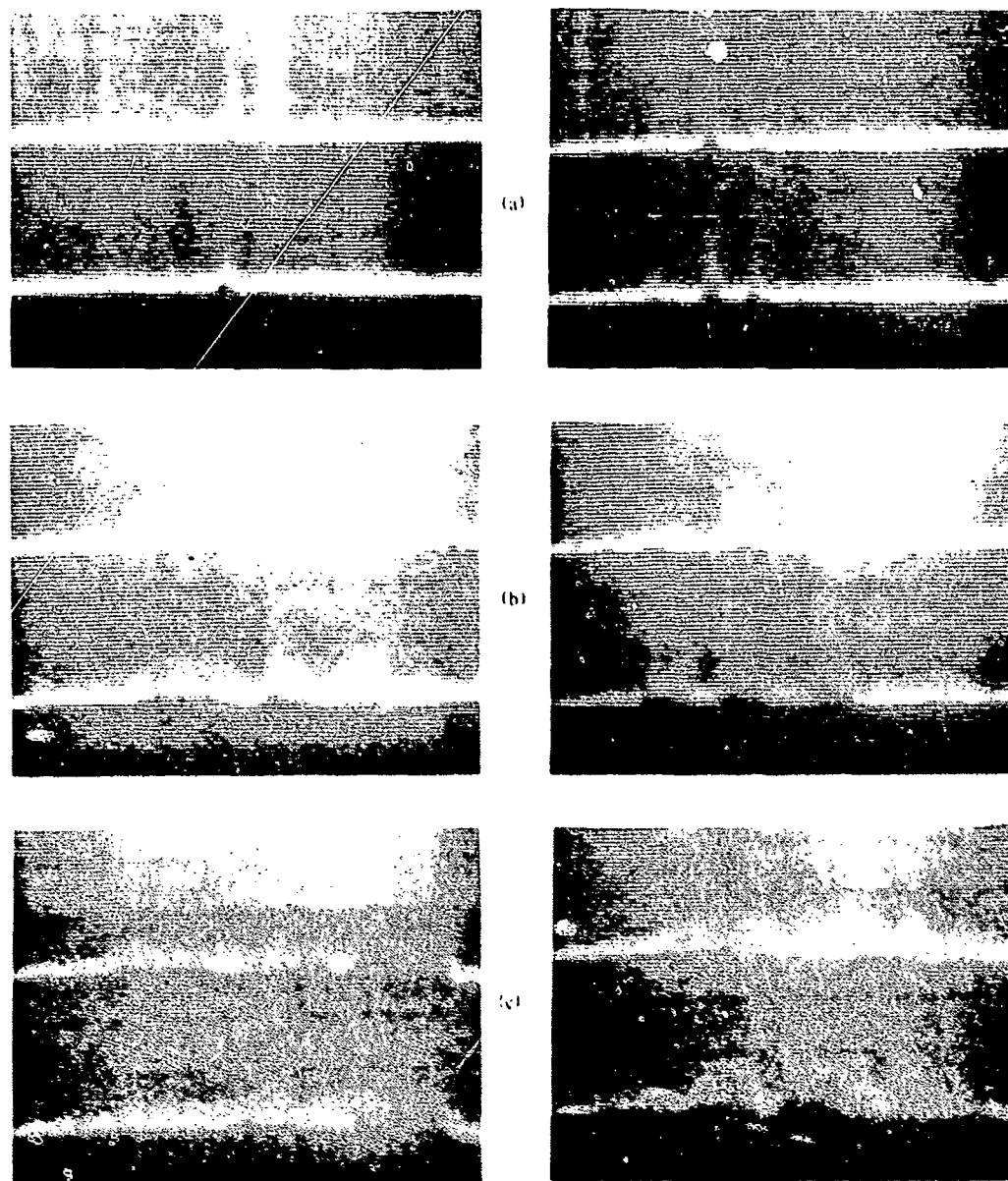
Fig. 16 — Typical A-scope displays in sea state 2 for pulse widths of (a) 40, (b) 200,
and (c) 400 ns, vertical polarization, time scale 200 ns per horizontal division

2   As in the shallow-water data, the returns were highly amplitude modulated, with modulation frequencies of the order of 20 Hz to more than 200 Hz. Figures 18 and 19 show examples of video spectral analysis vs time for approximately sea states 3 and 1 with vertical and horizontal polarization. It was noted during these tests that the pulse-modulation frequencies produced by breaking-wave crests were somewhat higher than the frequencies observed during the shallow-water Chesapeake Bay measurements. This difference is attributed to a difference in observation direction: the Chesapeake Bay
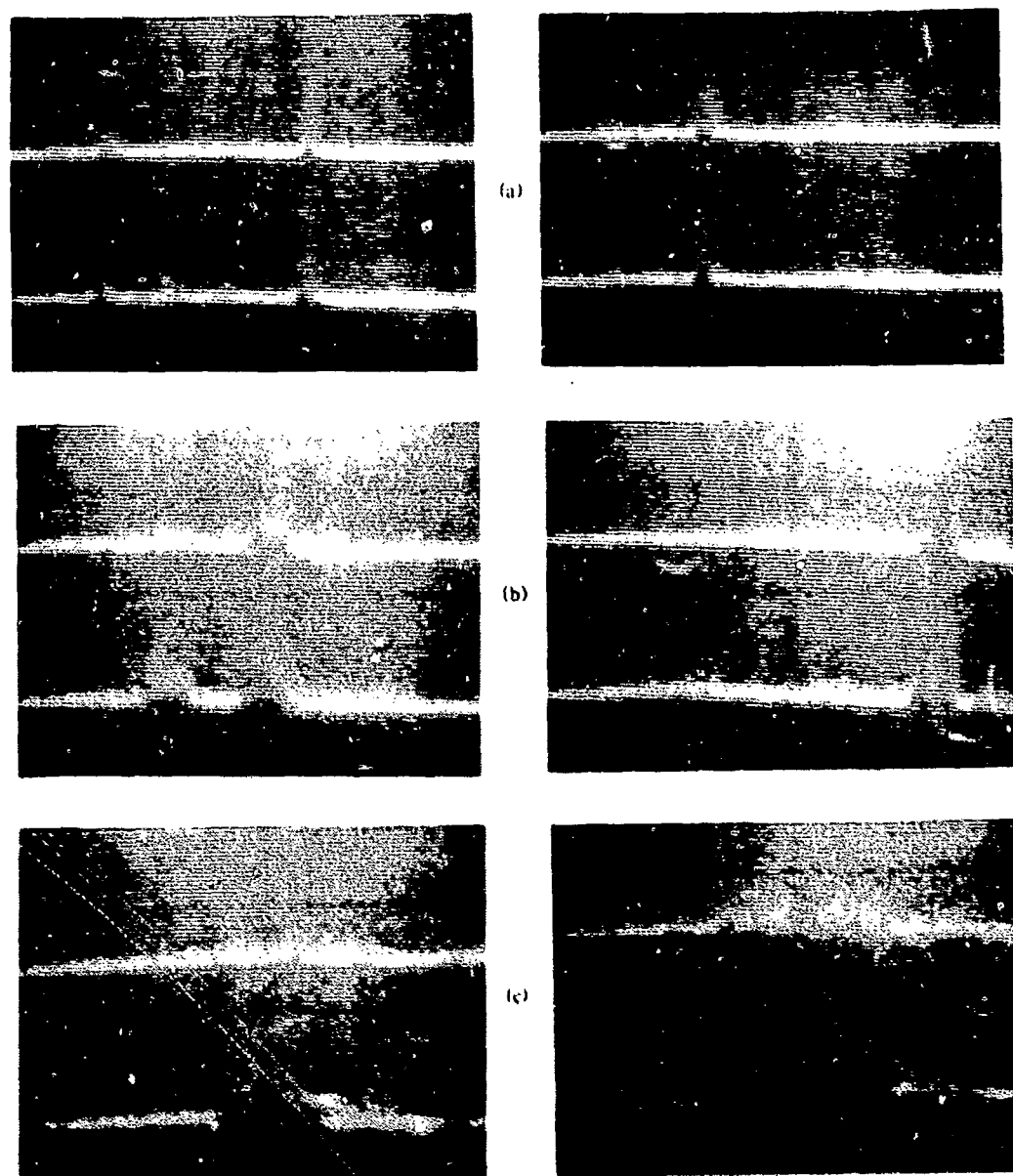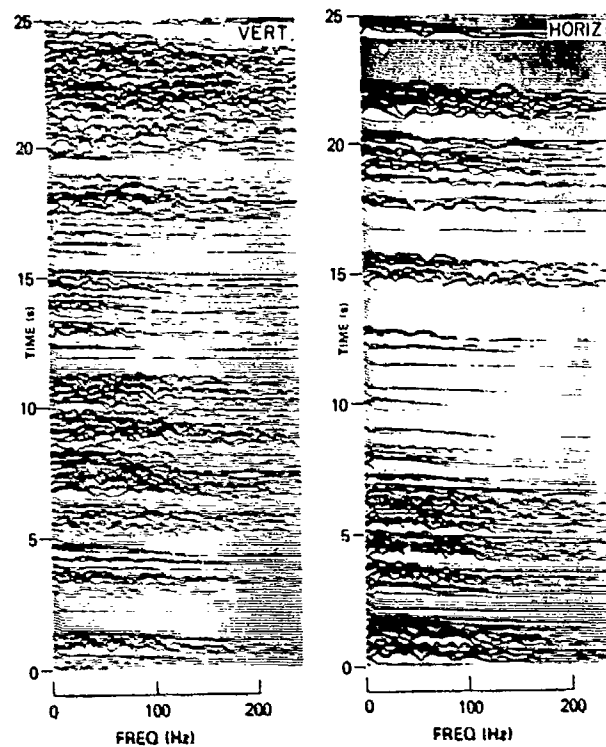
NRL REPORT 8557

Fig. 17 — Typical A-scope displays in sea state 2 for pulse widths of (a) 40, (b) 200, and (c) 400 ns: horizontal polarization, time scale 200 ns per horizontal division

measurements were primarily upwind along a normal to the breaking wave crests, whereas the Boca Raton measurements were partially crosswind at an angle of 45° to the normal. The higher modulation frequencies may have simply been a result of an apparent higher range growth rate of the breaking wave crests when they were observed from directions away from the normal to the crest

3. Polarization sensitivity was observed to be a function of both the water surface roughness and the alignment of wave crests relative to the line of sight. With slightly rough, unbroken water (sea states 1 or 2), vertical polarization yielded smaller but more frequent peaks than horizontal. When whitecaps appeared, the peak scatter amplitudes tended to be essentially independent of polarization (This was true unless the radar observation was nearly perpendicular to the wave crest. Then, as
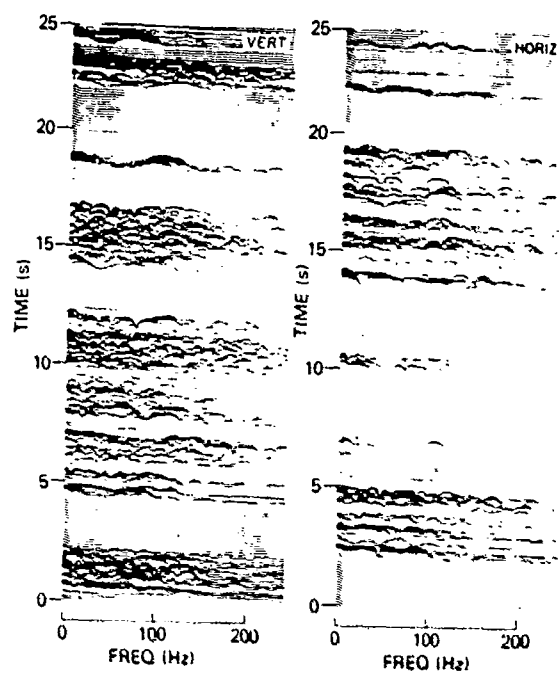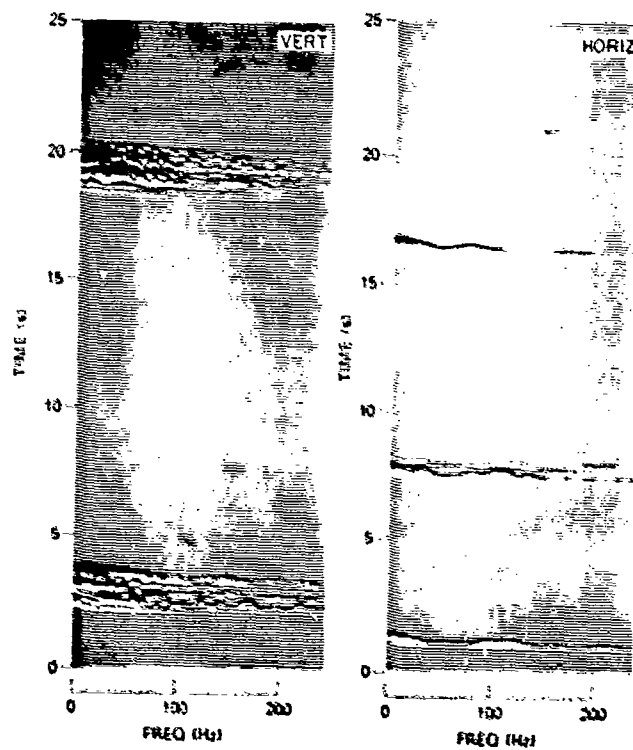
19

(a)
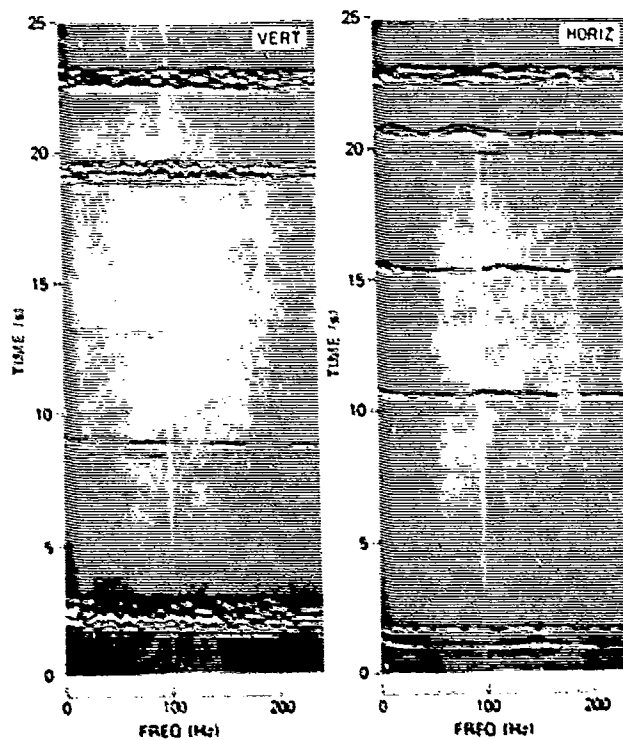
(b)

Fig. 18 — Video spectral analysis vs time for sea state 3
(a) 400-ns pulsewidth; (b) 40-ns pulsewidth

(a)

(b)

Fig. 19 — Video spectral analysis for sea state 1
(a) 600-ms pulsewidth, (b) 40-ns pulsewidth

observed in the shallow-water measurements, the backscatter with vertical polarization was sometimes greater than the backscatter with horizontal polarization.) Greater polarization differences were observed in connection with the duration of the spikelike intervals and their fluctuation. As seen in the data of Figs. 13 through 19, scatter returns occurred more frequently with vertical polarization and persisted longer. Moreover, when the line of sight was perpendicular to the wave crests, the backscatter with vertical polarization tended to follow the wave in range, whereas with horizontal polarization the scatter often tended to develop and disappear at the same range. Since the duration of the horizontally polarized scatter signals was generally shorter than that of the vertically polarized scatter signals, the horizontal scatter appeared more spikelike in character.

Deep-Water Data (30.7-m Depth)

The single-frequency, contiguous-range-cell measurement system was used to make deep-water measurements at Stage I (see Fig. 20), 16 km (10 m) offshore from Panama City, Florida. In these measurements the 2.67-m (1° beamwidth) antenna was employed. The antenna was mounted 15 m above mean sea level, and the center of the beam was aimed to intercept the water at a distance of 300 or 600 m. This produced a grazing angle of 3° or 1.5°. The 300- or 600-m range and 1° beamwidth produced azimuth resolution of 5 or 10 m, and the 40-ns transmitted pulse yielded a range resolution of 6.2 m (cell area was 31 or 62 m^2). It was noted at this open-sea site that for low wind and sea conditions there were often many small crests appearing on the sea surface which were relatively random in alignment (not necessarily aligned perpendicular to the dominant wind and wave direction). In cases of relatively high wind and sea conditions, a dominant crest alignment becomes more apparent, but even in these cases many of the smaller crests are still randomly oriented. Figures 21 and 22 show typical video data obtained at this site in approximately sea states 5 and 2 with vertical and horizontal polarization.
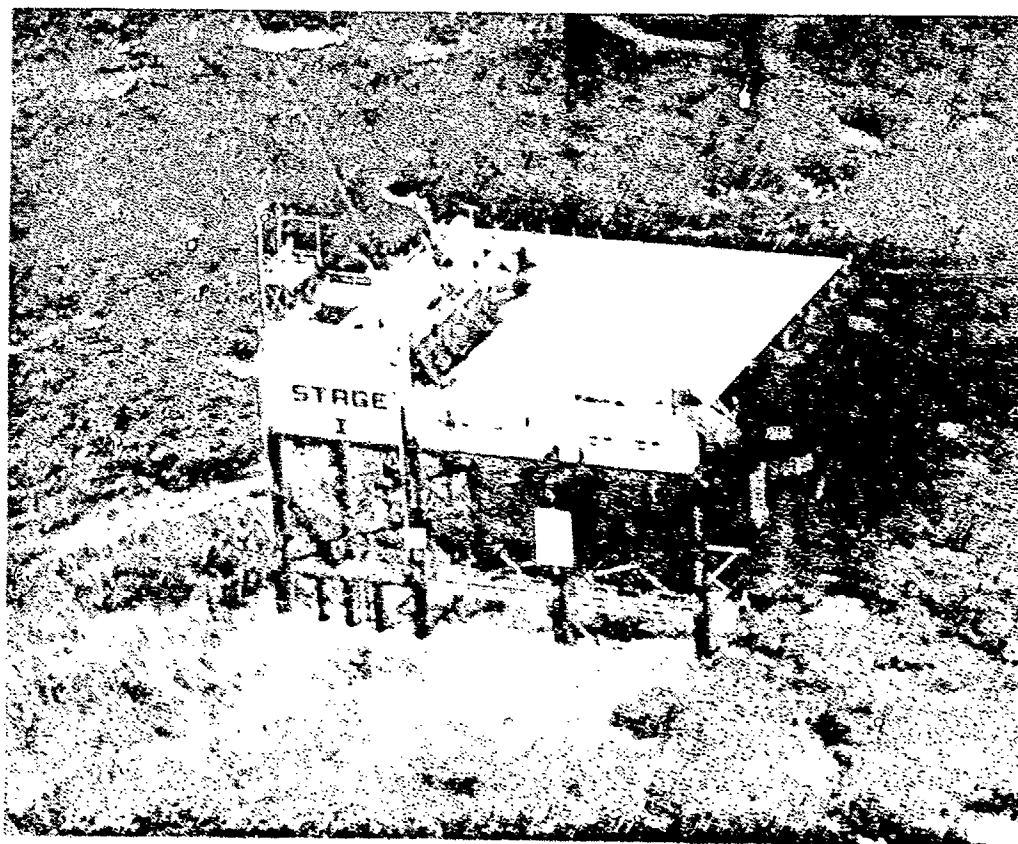

Fig. 20 — Measurement site deep-water data, Stage I, Panama City, Fla.

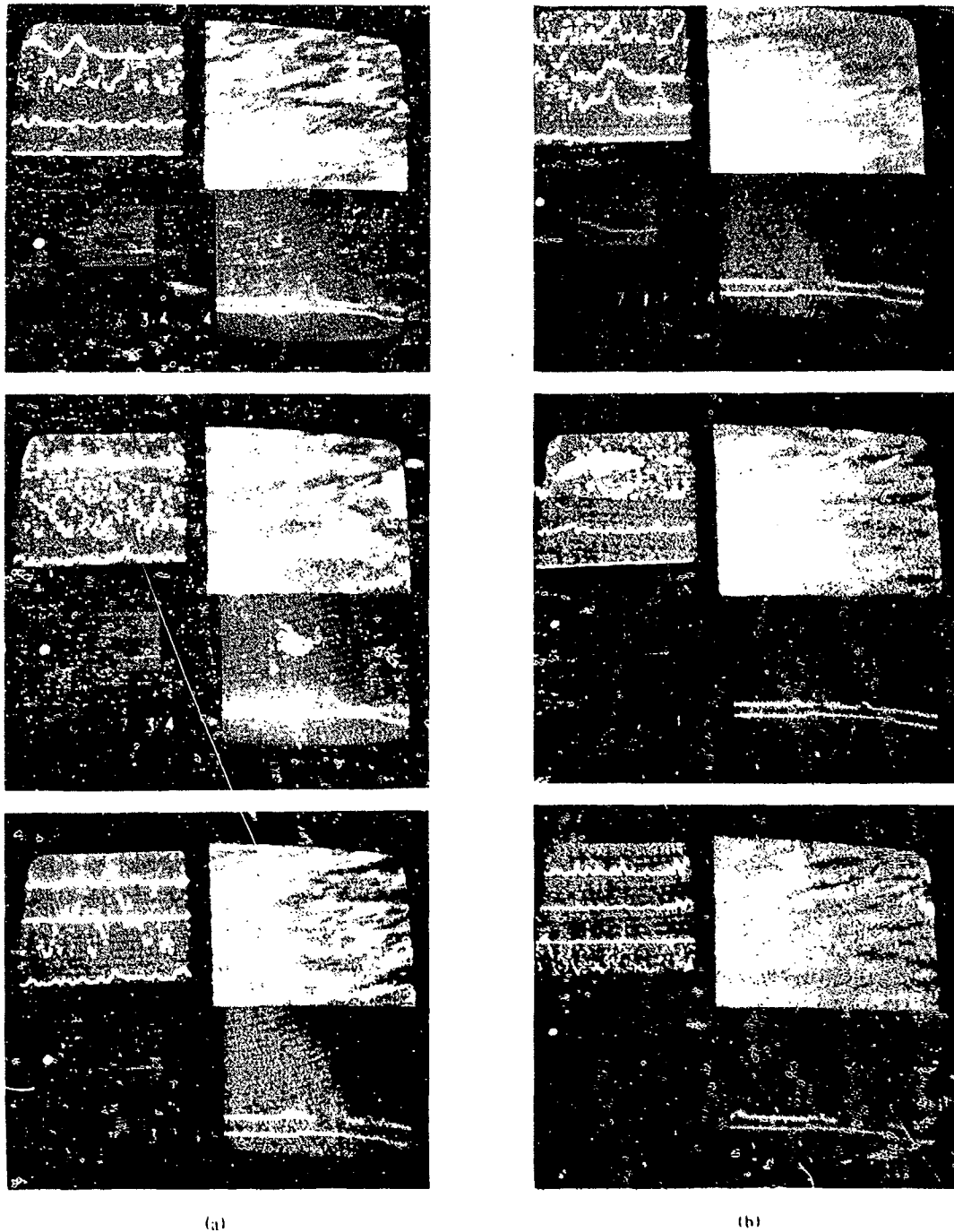(a)   (b)

Fig. 21 — Typical TV video data, deep water, sea state 5:
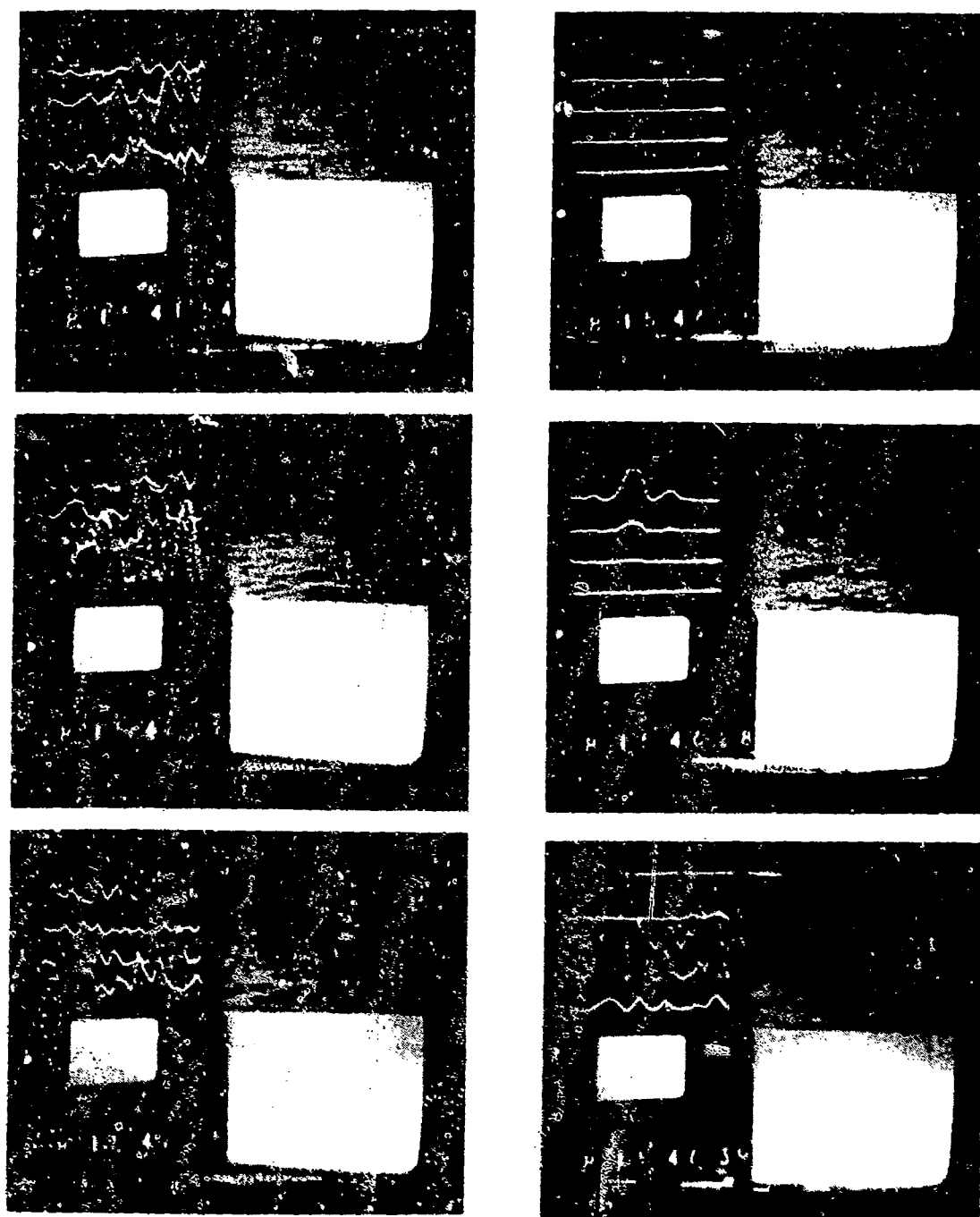(a) vertical polarization; (b) horizontal polarization

23

Fig. 5. Typical TV video data deep water sea state 3 (a) vertical polarization
(b) horizontal polarization

The measurements at the Stage I site once again reinforced the results from previous experiments. The contiguous-range-cell data also provided some insight into the spatial occurrence of the backscatter, especially as a function of radar polarization:

1. As in previous data, when returns were present in any range cell they were highly amplitude modulated pulse to pulse, with frequencies of the order of 20 Hz and sometimes exceeding 500 Hz. Note the modulation envelopes displayed in the video data of Figs. 21 and 22. The rise and fall times of these modulation envelopes are occasionally fast enough to define individual pulse intervals (as dots) in the sample hold display. Figure 23 illustrates a particular example of extremely high frequency pulse-to-pulse modulation. In this example (sea state 5, upwind, 3° incidence, horizontal polarization) the boresight is centered on a churning wave crest. Although it is not evident in the still photos, a review of the real-time TV video reveals an abrupt cross-range physical movement in a part of the observed wave crest. The pulse-to-pulse modulation envelope at several points during this movement is changing with peak to null spacings comparable to a single interpulse interval (0.4 ms). This example represents a pulse-to-pulse modulation frequency well over 500 Hz.

2. The backscatter at this high resolution (40 ns) has a noticeably spikelike appearance, with periods of extremely low level returns interspaced between relatively high level returns. Examples of this behavior for several sea states, incidence angles, and observation directions are shown as contiguous-channel, amplitude-time (24-s span) histories in Figs. 24 and 25. Note the range resolution of apparent scatter centers.

3. In the sea states tested, peak cross-section values greater than 10 m^2 were observed in individual range cells. They were generally associated with higher sea states and rough breaking water (whitecaps). Between breaking wave crests and under calmer sea conditions the backscatter often showed similar spectral content but with amplitudes of the order of 20 dB below 1 m^2. Amplitude distributions (plotted on Rayleigh statistical paper) for several 80-s data samples of sea scatter under different sea conditions are shown in Figs. 26 through 28. These distributions can be compared with a typical Rayleigh linear curve shown on each plot and also with the response of the data sampling system to filtered test noise, shown in Fig. 29.

Median cross-section values $\bar{\sigma}_0$ in decibels below one square meter per square meter (dB m^2) for the nominal upwind sea states 5 and 2 are compared in Table 1 with data published by other researchers. The measured values with vertical polarization are in reasonably good agreement with those compiled by Sittrop [4] and by Long [5] for similar sea conditions but lower resolutions. The measured horizontal-polarization values, however, are somewhat low. The higher resolution of the Stage I system (40 ns vs 200 to 400 ns for the published values) may in itself account for the difference.

Several trends are apparent from the shapes of the distributions. First, the curves tend to be linear on an exponential scale but have a falloff slower than a typical Rayleigh distribution for both polarizations at the higher sea states. Second, the curves become less linear at the lower sea state with horizontal polarization showing a distinctive bow or inflection in the distribution. These trends are similar to ones observed by Bishop [6] for measurements at 70-ns resolution. Long [7] has also cited data (at 6.3 GHz, 190 ns, horizontal polarization) with a break or bow in the distribution.

A polarization sensitivity with sea state and with crest alignment was very evident in the data taken at Stage I. In the low sea states vertical polarization tended to yield smaller but more frequent peaks than horizontal. In higher sea states, with rough broken water, the scatter peaks tended to be similar for both polarizations. For upwind conditions, backscatter with vertical polarization tended to follow the wave range while scatter with horizontal polarization tended to be sporadic.

Particularly prominent in the 24-s amplitude-time histories of Figs. 24 and 25 are "Kalmykov bursts" produced with horizontal polarization (a few of these bursts are designated in the figures). This

T = 0

(a)

T = 0.18 s

(b)

500 Hz TEST SIGNAL

0.02 s

CH 4

CH 3

CH 2

HIGH FREQUENCY MODULATION
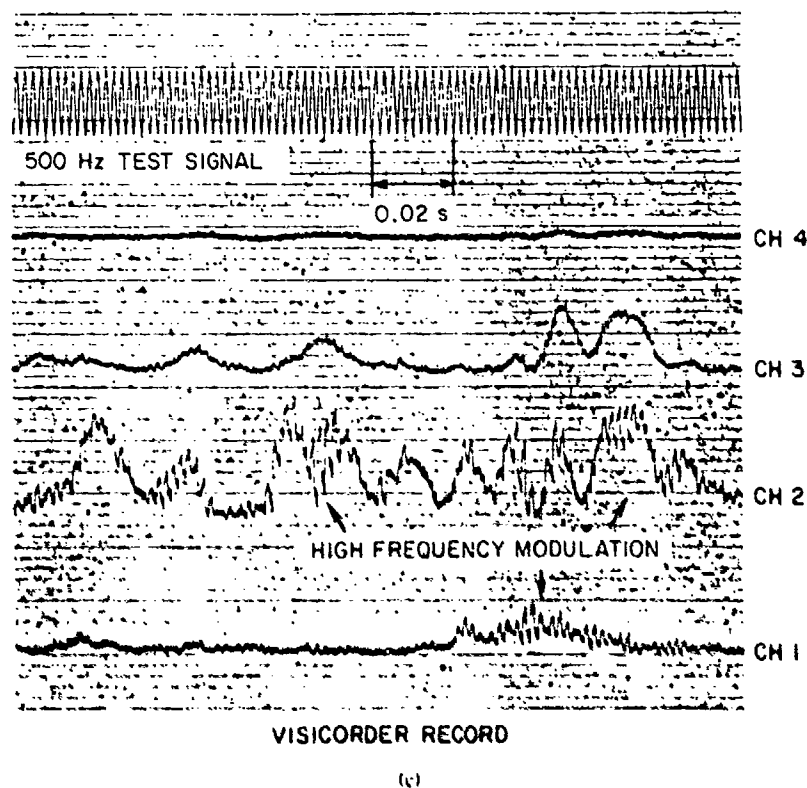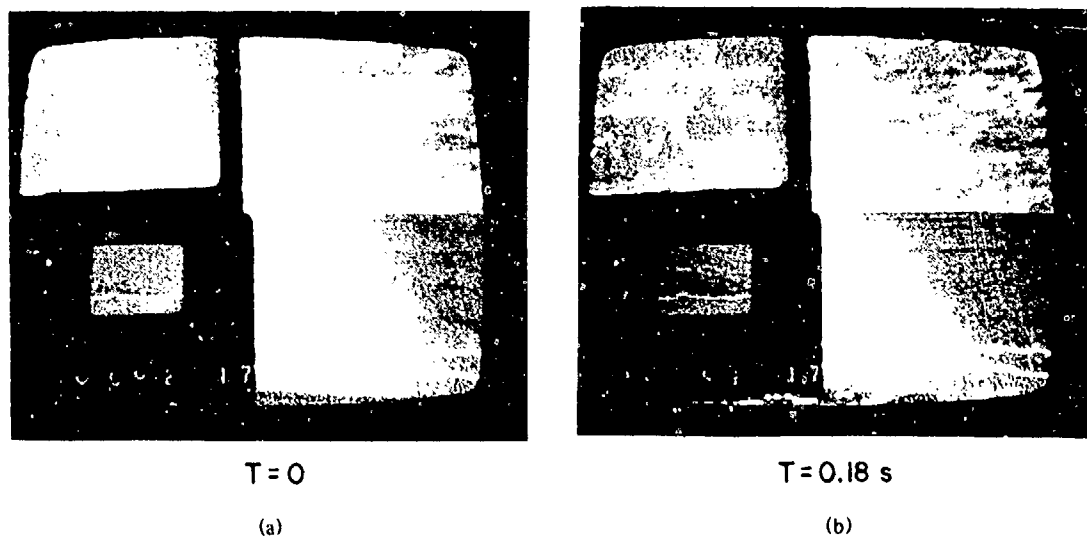
CH 1

VISICORDER RECORD

(c)

Fig. 23 — Data example showing extremely high frequency pulse-to-pulse modulation: (a) and (b) boresight photos taken 0.18 s apart; (c) visicorder record shows sampled and held scatter return in channels 1 thru 4 plus directly converted 500-Hz test signal. Sea state 5, upwind, 3° incidence with horizontal polarization.
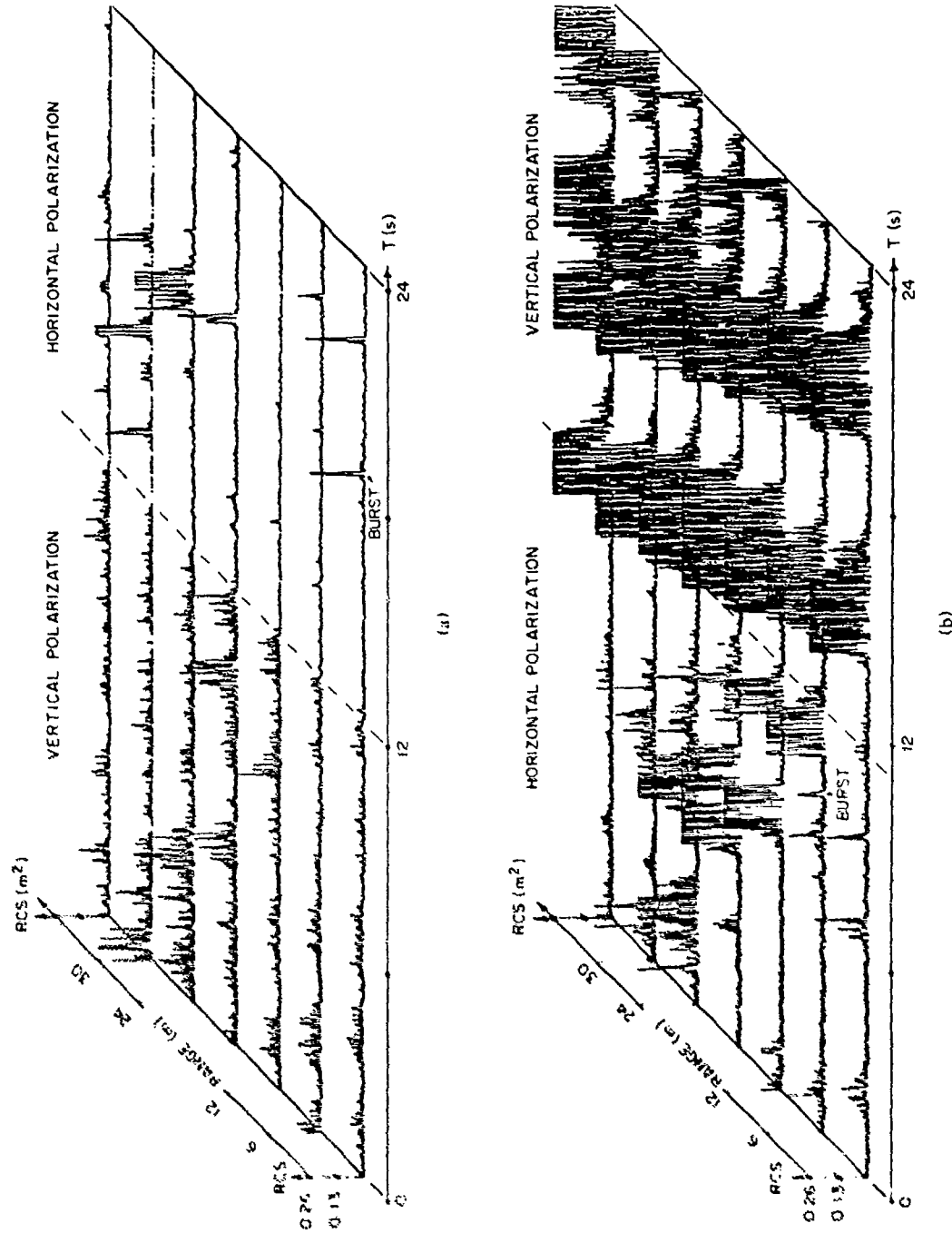
Fig. 24 — Backscatter amplitude-time history for seven contiguous range cells spaced 6 m apart. Data record length 24 s, 40-ns pulsewidth. (a) sea state 2, winds 8 knots, upwind, 3° incidence angle; (b) sea state 5, winds 22 knots, upwind, 3° incidence angle
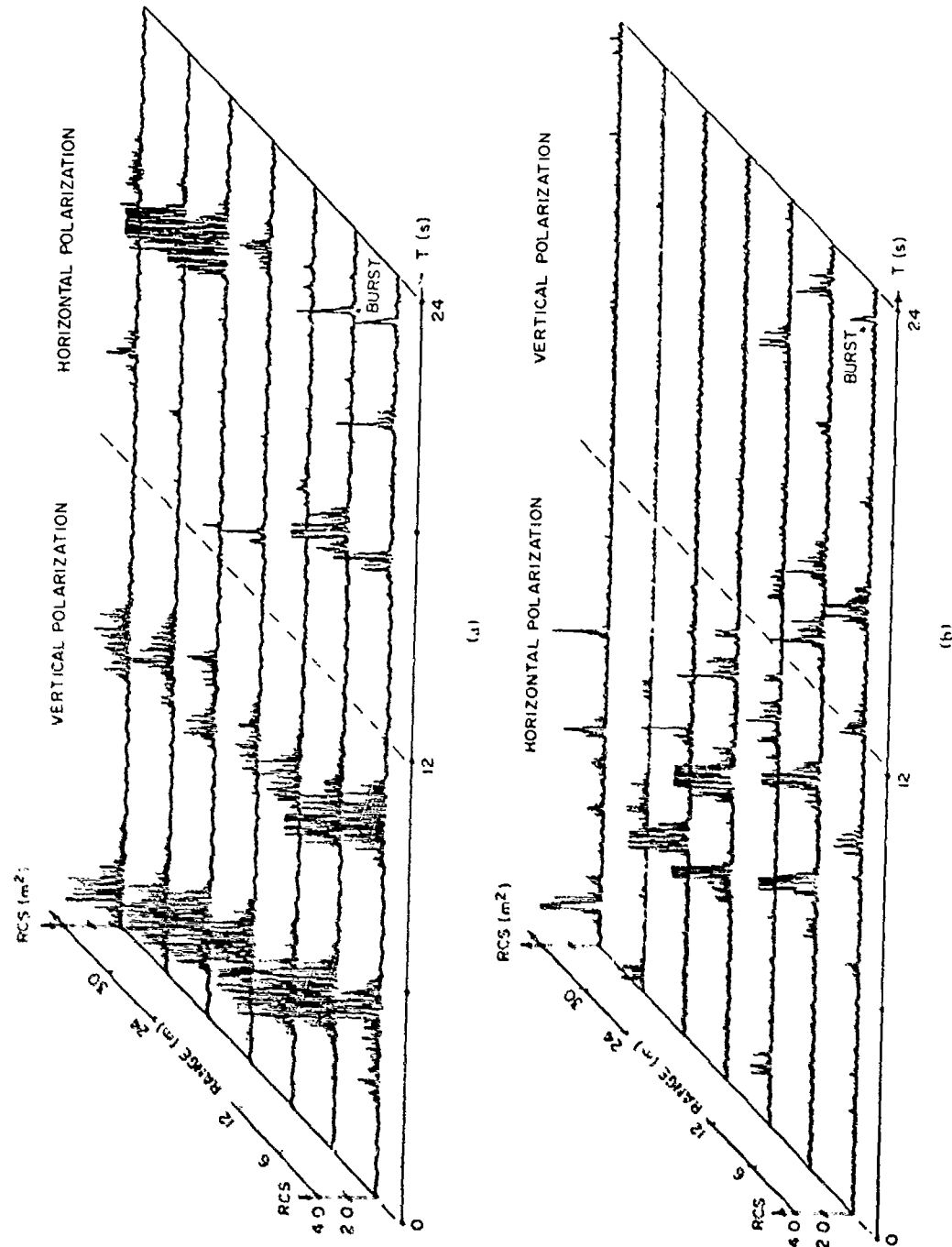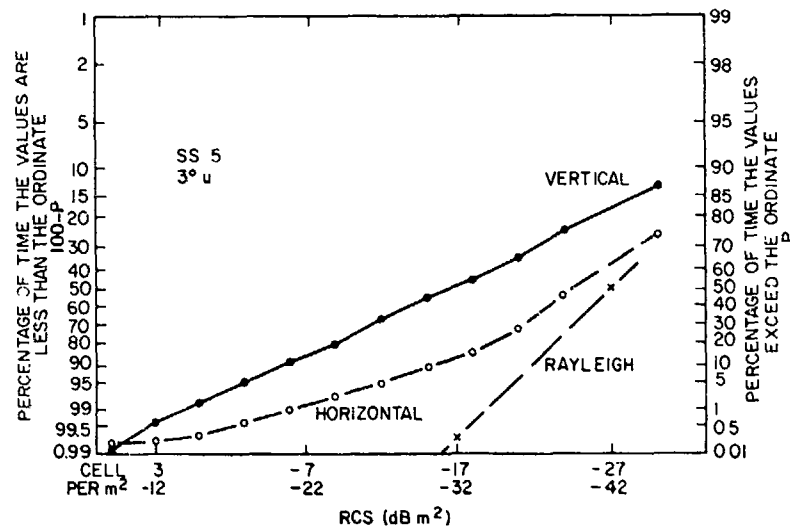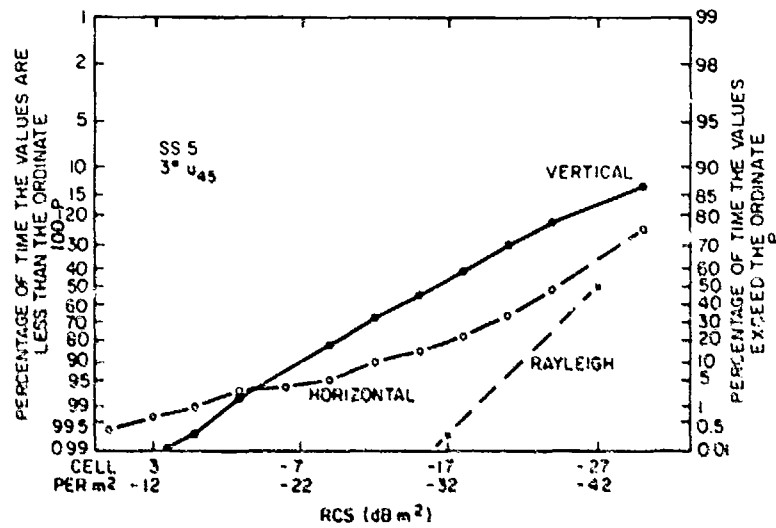
Fig. 25 — Backscatter amplitude-time history for seven contiguous range cells spaced 6 m apart. Data record length 24 s, 40-ns pulsewidth: (a) sea state 4 to 5, winds, 20 knots, upwind, 1.5° incidence angle; (b) sea state 3, winds 15 knots, crosswind, 1.5° incidence angle
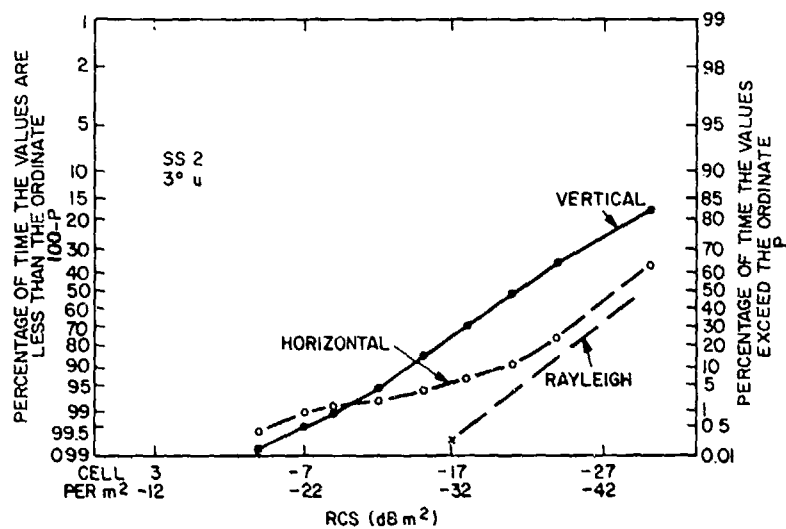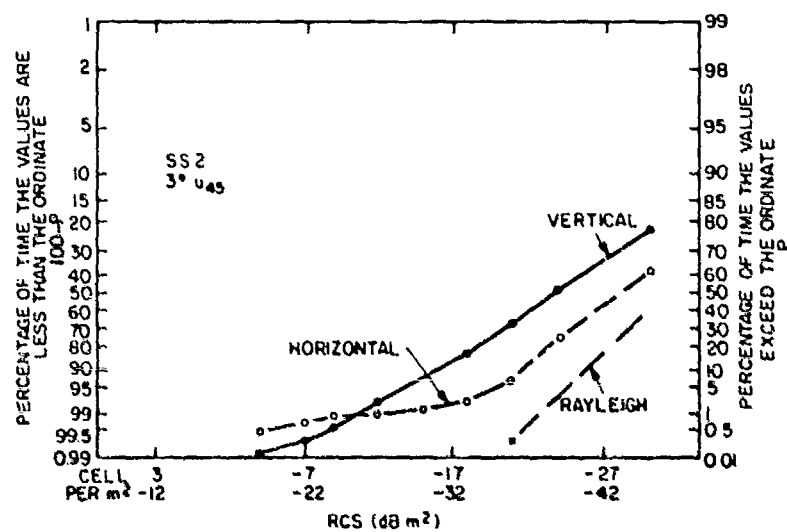
(a)

(b)

Fig. 26 — Amplitude distributions, sea state 5, 80-s time record (a) upwind
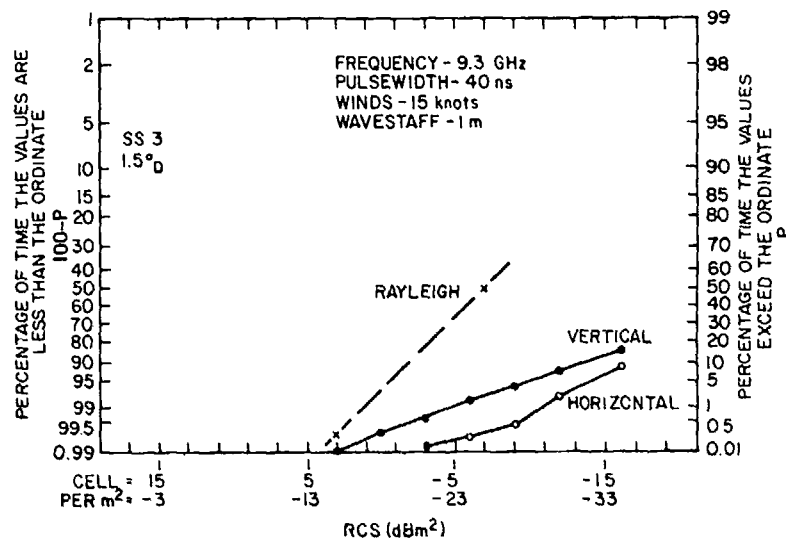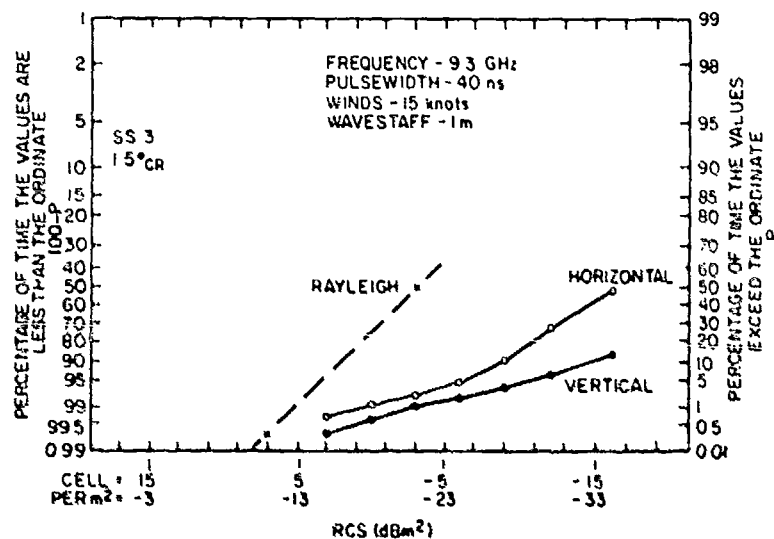and (b) 45° from upwind

(a)

(b)

Fig. 27 — Amplitude distributions, sea state 2, 80-s time record: (a) upwind
and (b) 45° from upwind

(a)

(b)

Fig. 28 — Amplitude distributions, sea state 3, 80-s time record:
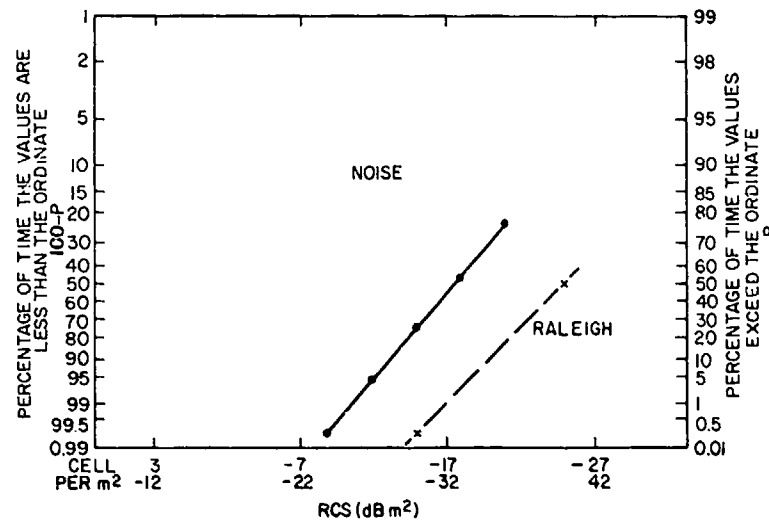(a) downwind and (b) cross wind (90°)

Fig. 29 — Amplitude distribution of filtered and rectified test noise.

Table 1 — Measured Upwind Cross-Section Values at X-Band

Researcher	Resolution (ns)	Wind (knots	Incidence (deg)	Median Cross Section	
				σ_{0_V} (dB m²)	σ_{0_H} (dB m²)
Hansen	40	22	3	−31.5	−39
Sittrop	120	22-26	3	−31*	−34*
Nathanson	500	19-24	3	−33.5†	−35†
Daley et al.	500	29	5	−35.5	−37
Guinard et al.	500	17	4	−36	−37
Hansen	40	8	3	−36	−43
Sittrop	500	10	2	−43*	−45*
Nathanson	500	7-12	3	−41†	−45†
Guinard et al	500	7	4	−38	−39
Bishop	270	8	1	−42*	−44*

*Median value obtained by subtracting 3.0 dB from average value as per Long [5].
†Adjusted median values where upwind, downwind, and crosswind results were averaged.

type of modulation was first noted by Kalmykov et al. [8] when observing the modulation envelope of scatter upwind from strongly breaking waves. These bursts were found to be present in virtually all of the Stage I data taken with horizontal polarization. In contrast, a burst formation was rarely observed with vertical polarization. An exception appears in the crosswind vertical polarization example shown in Fig. 25(b), where a few isolated burst modulations are present. In higher sea states, the scatter for horizontal polarization becomes a combination of relatively short duration but low frequency modulated bursts and relatively long duration but high frequency modulated spike returns (similar to the ones observed at Chesapeake Bay and Boca Raton from turbulent breaking water).

Consider the upwind 5-min data runs shown in Fig. 30. A comparison of a wave staff recording and the scatter data indicates that scatter with vertical polarization profiles every approaching wave while many of the waves are missed with horizontal polarization. Also note that the envelope formed
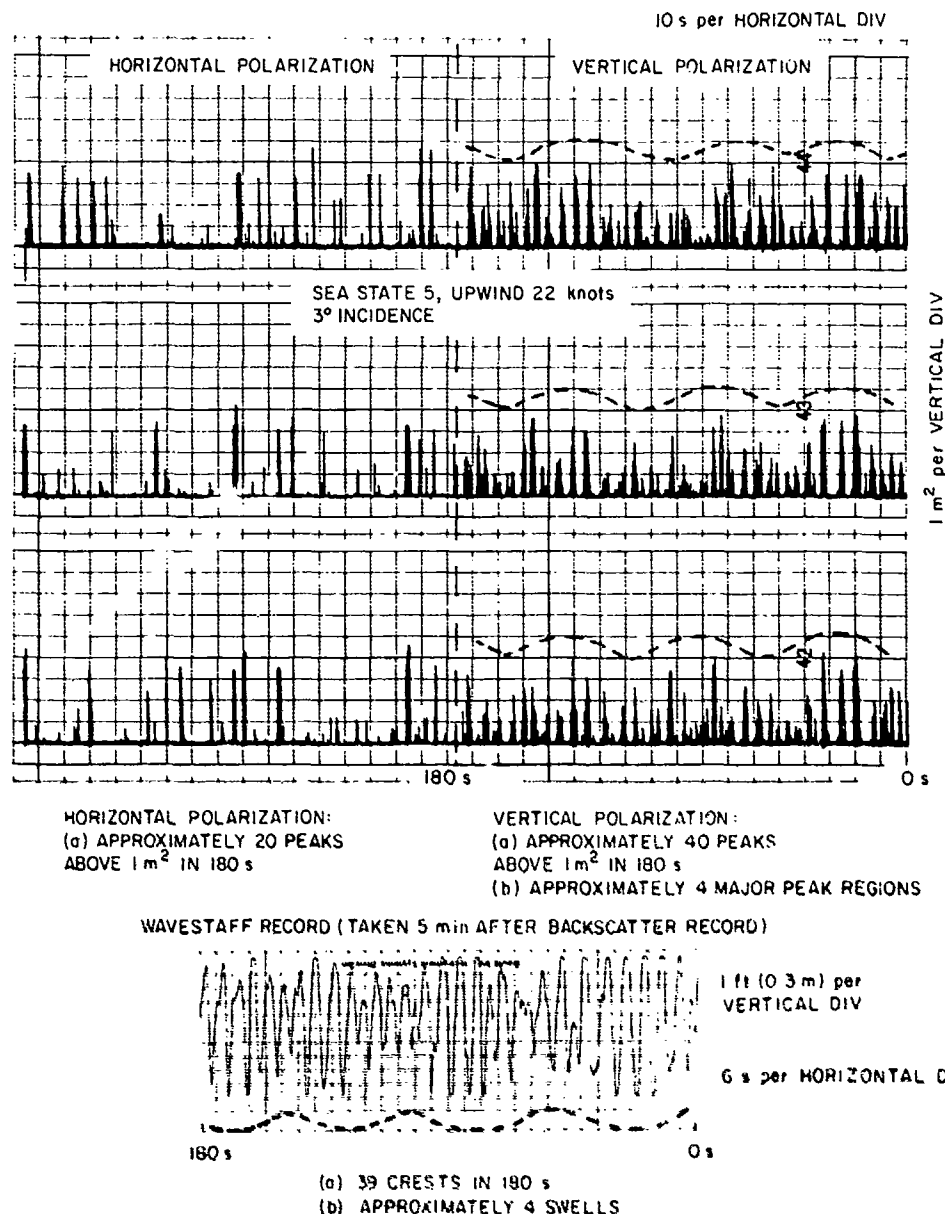
BACKSCATTER RECORD (CH 2,3,4)

Fig. 30 — Comparison of the scatter amplitudes in three contiguous range cells with a record of wave height and frequency of occurrence. (Wavelength record was taken 5 min after the backscatter record.)

by the peak scatter amplitudes for vertical polarization shows a slow periodicity, which is similar to the swell period present in the wave staff recording. It appears that for upwind conditions and vertical polarization the radar is receiving scatter from contributing features which are present on all of the unshadowed wave surfaces, while with horizontal polarization only very specific and range-resolvable features are producing scatter.

Kalmykov and Pustovoytenko [9], Long [10], and others have suggested that one of the dominant scatter sources for vertical polarization is small waves or ripples, while a dominant scatter source for horizontal polarization may be facets or sharp wave crests (or "wedges"). These suggestions would seem to explain the observed profiling action of the return for vertical polarization, since small ripples would be present on virtually all of the nonbreaking wave surfaces. Occasionally occuring sharp crests

could also be the source of the burst modulations seen in scatter data taken with horizontal polarization. However, the fact that the burst modulations do not appear for every wave formation would also indicate that there might be preferential alignment or shape needed to produce the scatter. Lewis and Olin [3] have suggested that some of the scatter is caused by sharp wave crests acting as impedance discontinuities. They speculate that the scatter from the crests should be preferential, with vertical polarization scatter being optimized for crest alignments normal to the radar and with horizontal polarization scatter being more probable for crests aligned away from the normal. These suggestions may have some confirmation in the observed differences in the amplitude distributions shown in Figs. 26 and 27. The distributions show a definite decrease in the peak vertical return and an increase in the horizontal return when the observation direction is changed from normal to 45°. There have also been occasional instances of sea states and observation directions where the scatter for horizontal polarization is substantially stronger than that for vertical polarization. (Note the data shown in Fig. 28.) Finally, there has been general agreement by previous researchers (Long, Kalmykov, and Bishop), as confirmed by the data in this report, that turbulent breaking water is associated with a characteristic high-level scatter which appears to be similar in magnitude and in modulation for both polarizations. A net observation is therefore reached that radar scatter at high resolution may, in fact, be produced by many types of resolvable surface formations, with ripples, sharp crests, and regions of turbulent breaking water being at least three that are evident.

THEORETICAL MODELING OF THE SCATTER SURFACE

As outlined by Lewis et al. [1-3], modeling results have suggested that the temporal characteristics of the sea backscatter might be approximated by a surface containing random amplitude and phase zones spaced at quarter-radar-wavelength intervals (Fig. 31).

Simple addition or subtraction of scattering zones (as in the formation and decay of a whitecap) results in a characteristically rapid modulation. Several sea-spike realizations with different relative internal and external correlation times are shown in Fig. 32. Comparisons of this computer modeling with experimental data have suggested that the internal and external correlation times of typical sea backscatter are of the order of 0.01 s at X-band. The modeling results were also extended to the cases when a slightly disturbed surface (as produced by wind or rain) fills the entire resolution cell.

As a further check on this type of model, a simple experimental simulation was made. This experiment utilized an oval-shaped roughened surface sliding on a tilted plate (see Fig. 33). The rough surface was steadily moved through the beam of the dual-frequency radar system in order to approximate the growth (and decay) of a turbulent sea surface. Figure 34 shows some examples of the backscatter pulse-to-pulse modulation characteristic produced by this experimental model. Note the similarity in the amplitude characteristic to actual scatter from the sea surface.

EXPERIMENTALLY OBSERVED SCATTERING CHARACTERISTICS OF RIGID TARGETS

The radar-echoing characteristics of some rigid targets were also observed in an attempt to establish possible discriminants which could be used against sea scatter. Examples of the scattering character of a submerged platform and a small floating target are shown in Fig. 35. The dominant difference between the backscatter from the sea surface and that from rigid targets was noted to be in the depth and modulation frequency of the pulse-to-pulse amplitude-modulation characteristic. In general, returns from rigid targets are found to have much lower modulation frequencies and percentage of modulation when compared to typical sea return.

As a contrast, the statistical distributions of the scatter from a floating 6-in (15-cm) metal sphere (in approximately sea state 1) and from the sea surface (at sea state 2) are compared in Fig. 36. Note that the amplitude distributions are very similar. A marked difference is observed, however, in a comparison of the pulse-to-pulse modulation characteristics shown in Fig. 37.
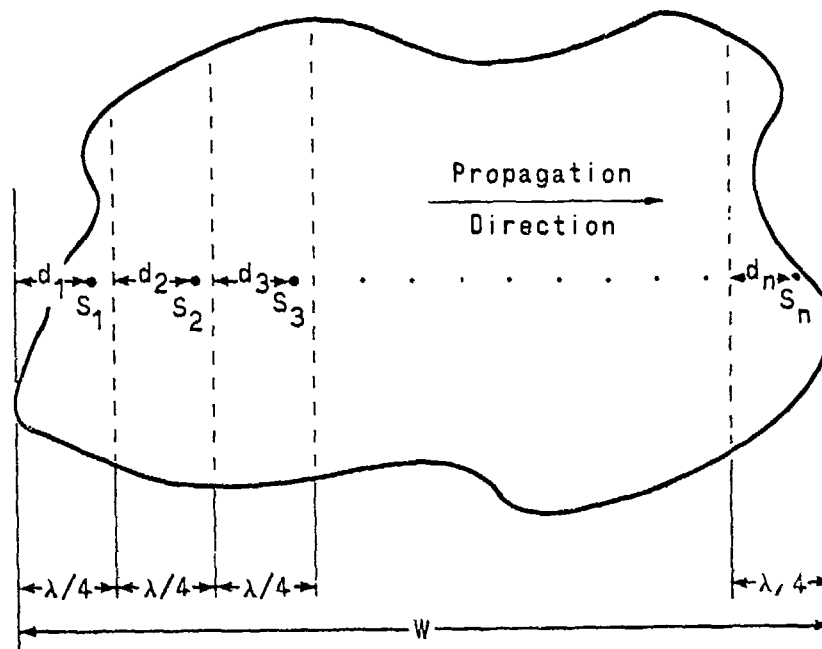
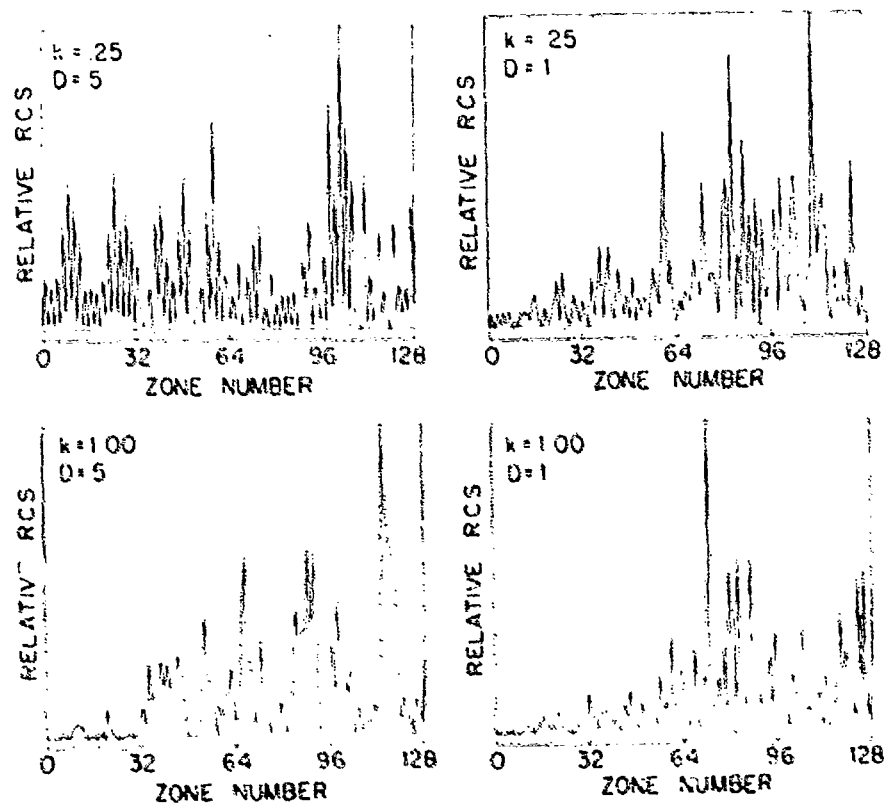Fig. 31 — Theoretical model of a disturbed sea surface

Fig. 32 — Computed simulations of sea-spike realizations for several internal and external growth and decay rates
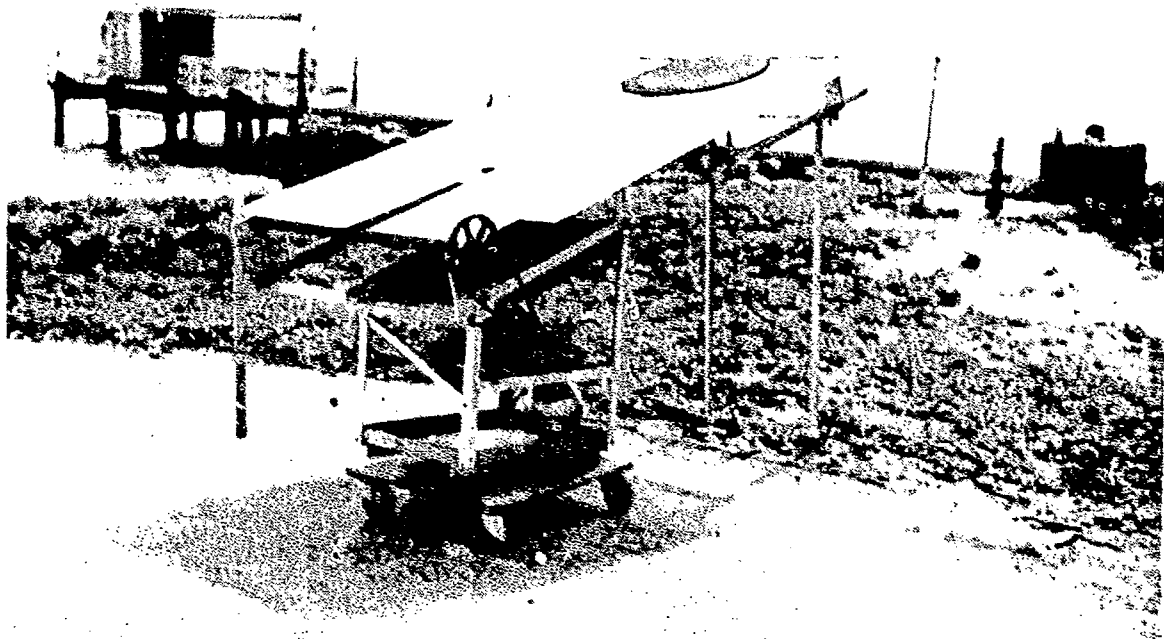
Fig. 11 — Experimental apparatus for a simulation of sea water "body" roughened surface sliding on a tilted conducting plate
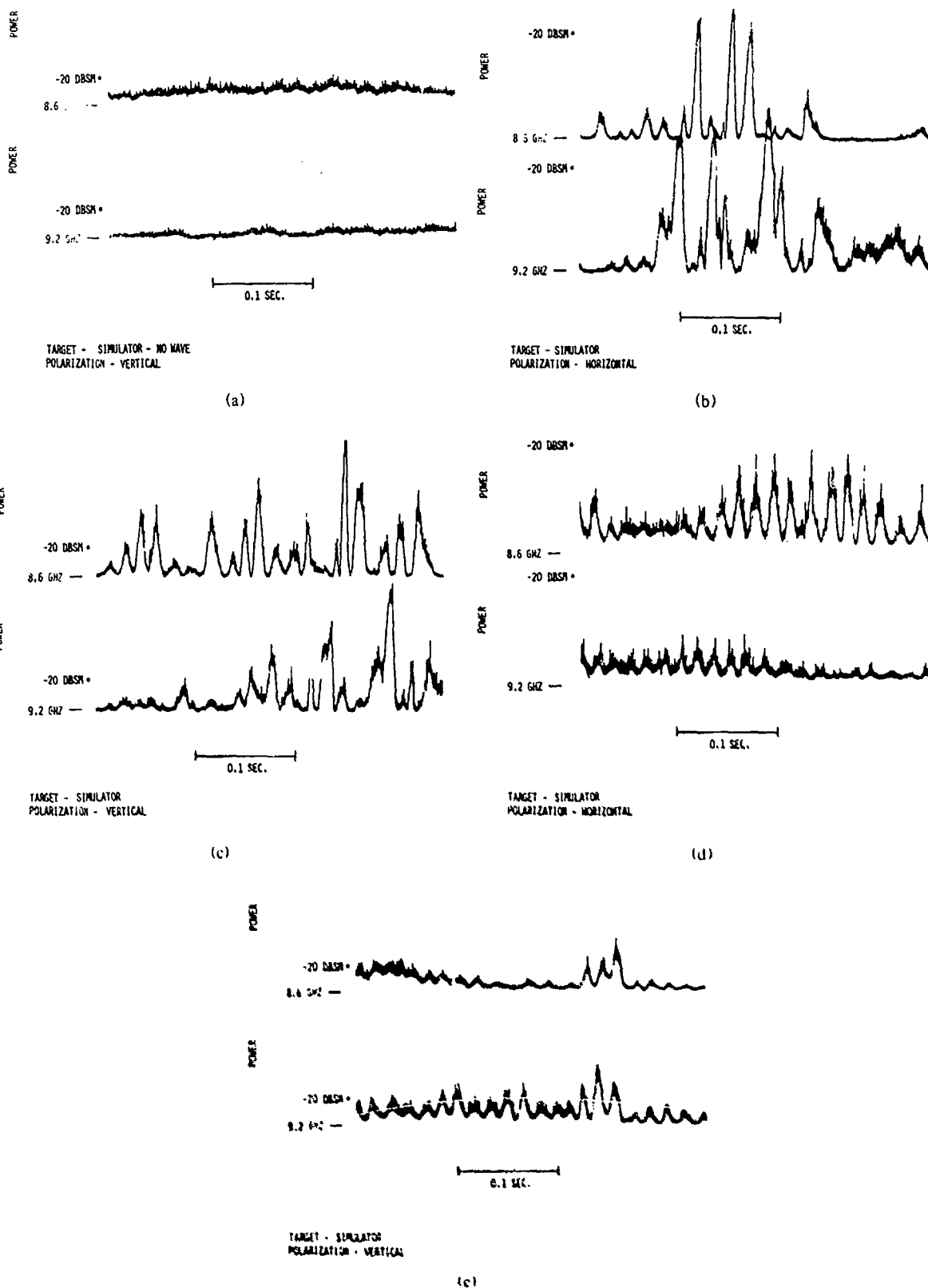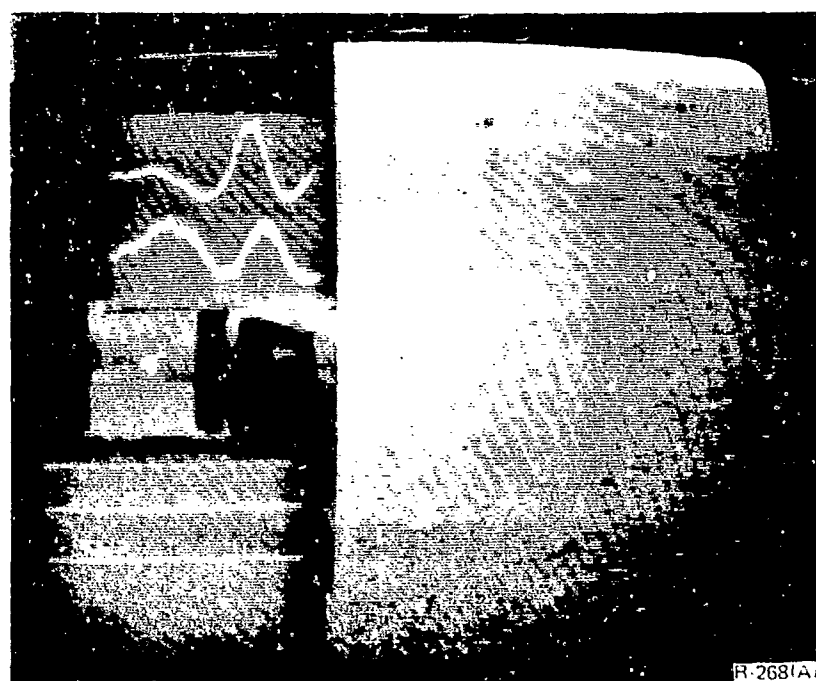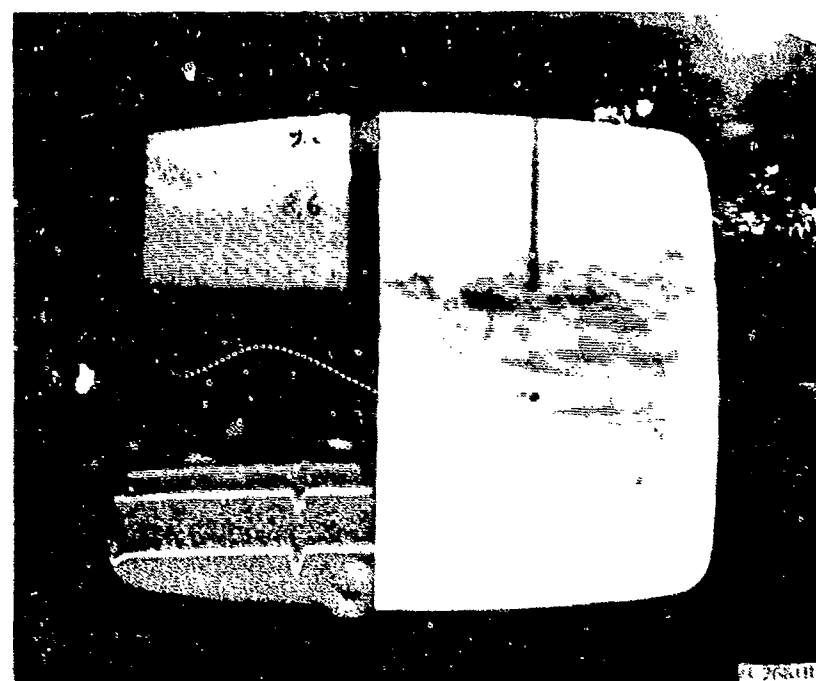
Fig. 34 — Pulse-to-pulse amplitude-time histories produced by observing the experimental simulation apparatus of Fig. 33 with a dual-frequency, high-resolution measurement system
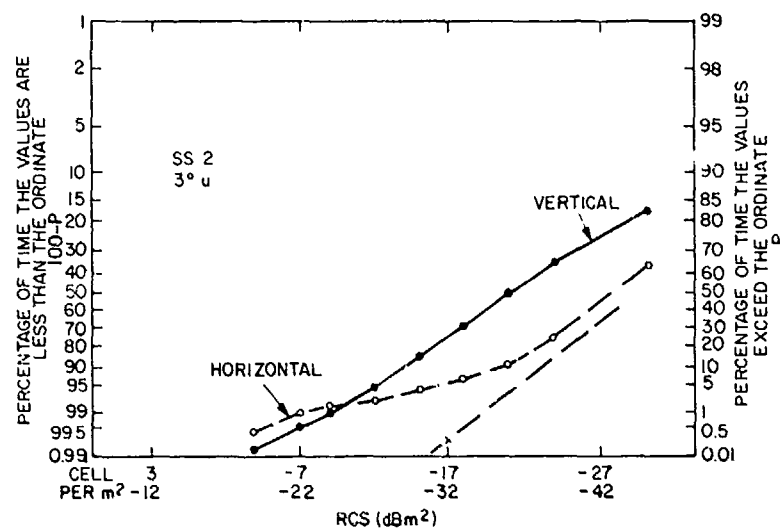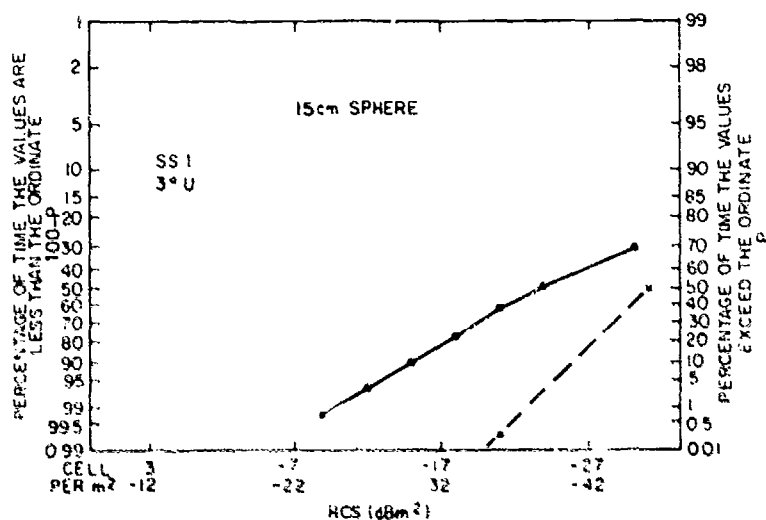
(a)

(b)

Fig. 35 — Typical TV video data, dual-frequency X-band system scatter from a floating corner reflector (a) and from a partially submerged wooden platform (b)

(a)

(b)

Fig. 16 — Comparison of the amplitude distributions of sea state 2 (observed from upwind) (a) and of a floating sphere in sea state 1 (b)
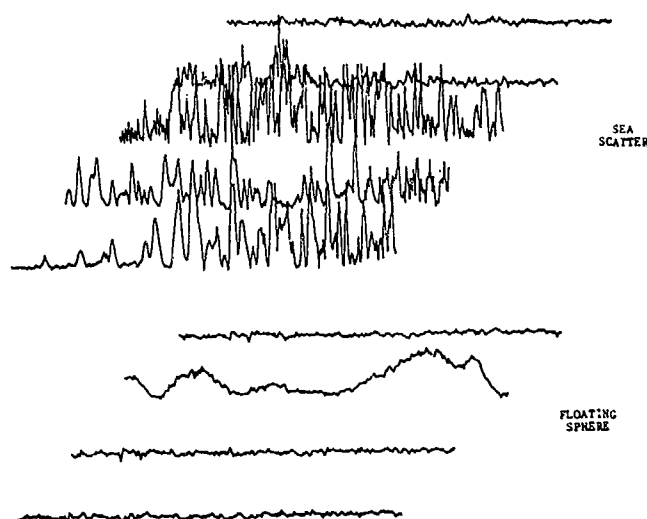
Fig. 37 — Examples of pulse-to-pulse amplitudes of scatter RCS from typical sea surface (a) and from a floating sphere (b) (data record 1 s)

SEA-SCATTER DISCRIMINANTS AND TARGET DETECTION HIGH-RESOLUTION RADAR

The difference in the amplitude-modulation characteristics of rigid floating debris and sea return suggests that percentage modulation vs time might be used as a discriminant to suppress sea return. Figure 38 illustrates one way in which such a discriminant can be instrumented. The radar return signals from individual range cells are delayed by selected intervals via sample/hold circuits. The outputs are subtracted from each other as indicated to detect high-frequency, large-percentage amplitude modulation on echoes in a given range-resolution cell. If such modulation is detected, the output from one or more of the subtractors will exceed a preset threshold and inhibit a gate to block passage of that video to a display. Since sea return generally fluctuates by more than 6 dB in less than 20 ms, and rigid target echoes often remain constant for much longer intervals, this type of instrumentation can block sea-return video and pass typical target video.

This blockage should not materially reduce the probability of detection of rigid targets as long as the high-amplitude sea returns are occurring for only a small amount of viewing time. Loss of target will occur when sea return and target return occur in the same cell (with that cell being blocked). For a reasonable detection threshold, however, this blockage should correspond to relatively small reductions in viewing time.
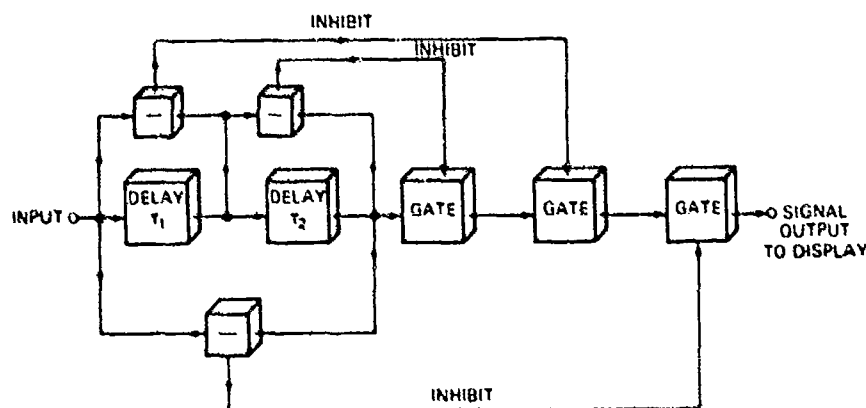
Fig. 38 — A sea-scatter rejection circuit based on amplitude-modulation characteristics of pulse-to-pulse scatter

40

As a means of testing the amplitude-modulation discriminant, recorded data from the contiguous-range-cell measurements of Stage I were utilized in several different experiments to demonstrate target detection and sea-scatter rejection.

In one test, an analog two-delay circuit was instrumented to operate on the recorded contiguous-range-cell data and display the results in unprocessed and processed range formats. In these tests target signals (simulated) were inserted in one range cell to observe target maintenance. Figures 39 and 40 illustrate typical results. Note that sea clutter is rejected and simulated target signal maintained with few false alarms or target rejections.

The Stage I data were also digitized and were processed by a five-delay rejection discriminant. The results are tabulated in Table 2. These tests indicated that for simulated target modulations below 5 Hz, a multiple-delay discriminator can effectively reject the sea scatter and maintain a target signal. As tested in this simulation, the five-delay discriminant performed best for individual delays of the order of 12 ms (60-ms total delay). A sea-spike false alarm (in the discriminator output) occurred only when the amplitude-modulation characteristic was obscured by system saturation.

SUMMARY OF EXPERIMENTAL RESULTS

The experimental measurement program has provided data which have led to the following observations concerning high-resolution-radar scatter from a disturbed sea surface and from rigid targets:

1. High-resolution X-band sea scatter observed from low incidence angles (less than 5°) is *always* heavily amplitude modulated with relatively high modulation frequencies. (Modulation frequencies on the order of 20 Hz to more than 500 Hz have been detected.) The frequency of modulation appears to be influenced by such parameters as the type of physical surface (breaking water, sharp wave crests, ripples, etc.), the relative wind and wave direction, and the radar polarization. Specifically, it has been observed that, for turbulent breaking water, higher modulating frequencies are observed (with both polarizations) in directions away from a normal to the dominant wave crest. This may simply be a result of the relative range growth rate of the turbulent area. In calmer seas, returns for horizontal polarization are dominated by lower frequency modulated Kalmykov bursts.

2. The time-varying characteristic of sea scatter is also dependent on transmitted pulse width. Low-resolution backscatter tends to appear continuously noiselike. As radar resolution is increased, the backscatter is punctuated by quiet periods and presents a spikelike characteristic with time (especially with horizontal polarization).

3. With high resolution, high-amplitude sea-spike returns often occur during the turbulent breaking action indicated by whitecap development. A spikelike characteristic can still be present during periods of relatively undisturbed sea, but the return is generally two to three orders of magnitude lower in power.

4. A polarization sensitivity is evident which is a function of both water roughness and alignment of wave crests to the radar system. In most (but not all) sea states and crest alignments vertical polarization tends to yield smaller but more frequent spikes. Also, when the scatter occurs, it tends to persist longer for vertical polarization.

For upwind conditions, in particular, return scatter with vertical polarization is evident from virtually all portions of the nonshadowed sea surface, while horizontal polarization produces sporadic returns, often with the burst character. These scatter modes may be an indication of some distinct physical scattering formations: small waves or ripples for vertical polarization and preferentially aligned sharp wave crests for horizontal polarization.
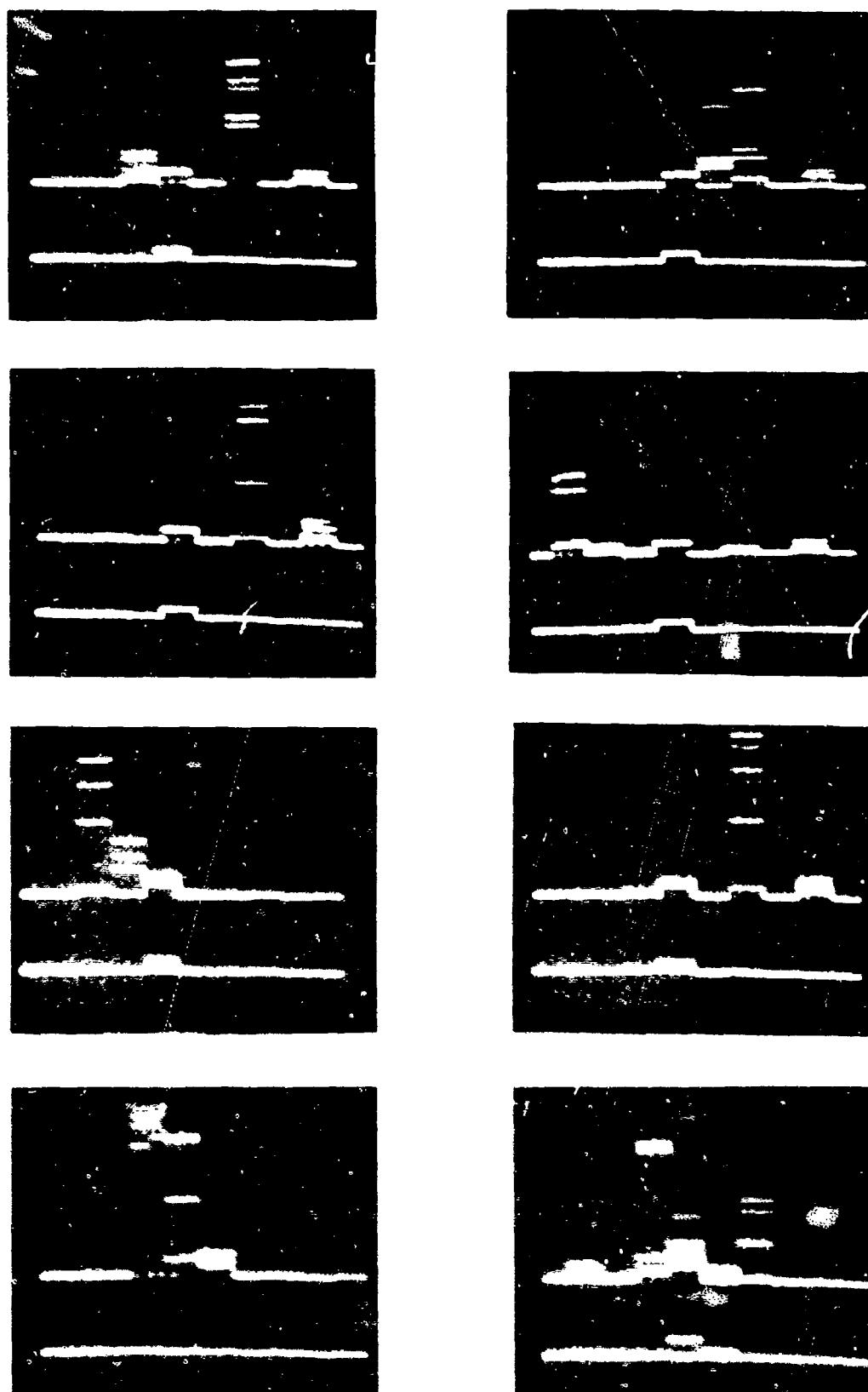
Fig. 19 — Performance of 3-delay sea-scatter rejection circuit (10-ms delays) on contiguous-range-cell data (constant-level simulated-target signal added to range gate 4). Top trace in each unprocessed, bottom trace processed
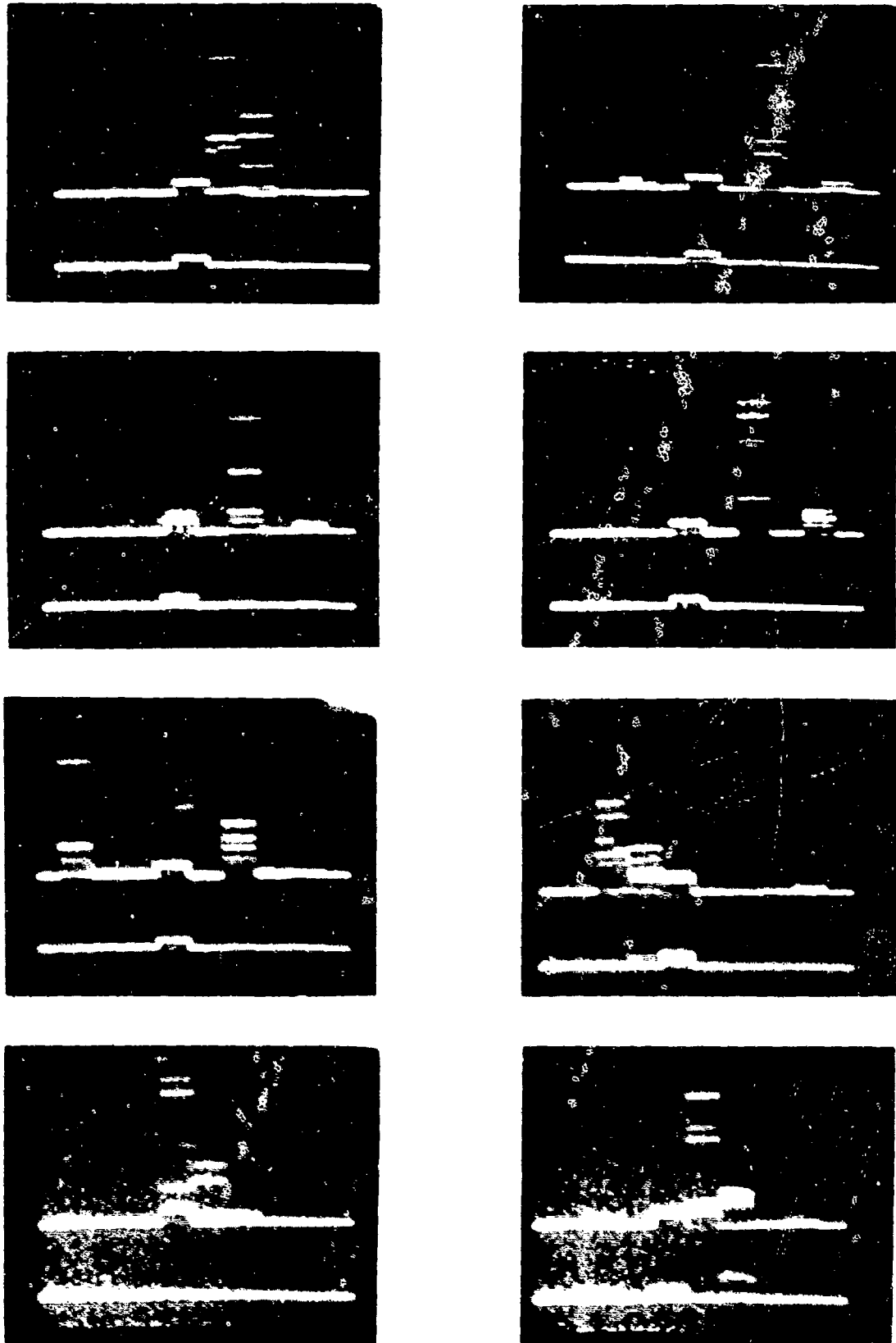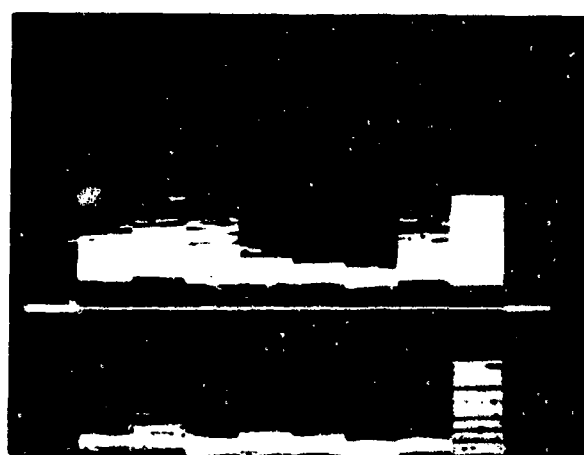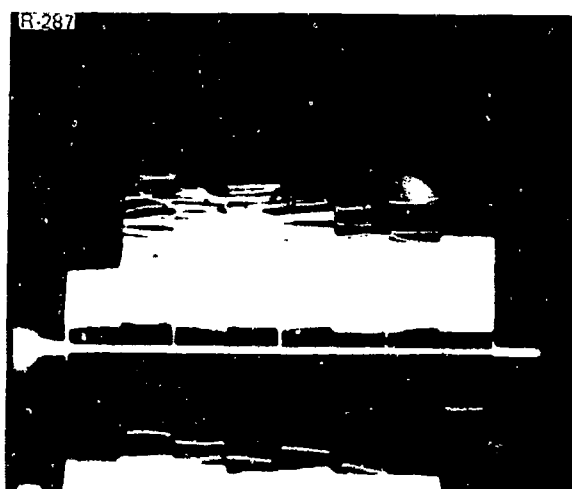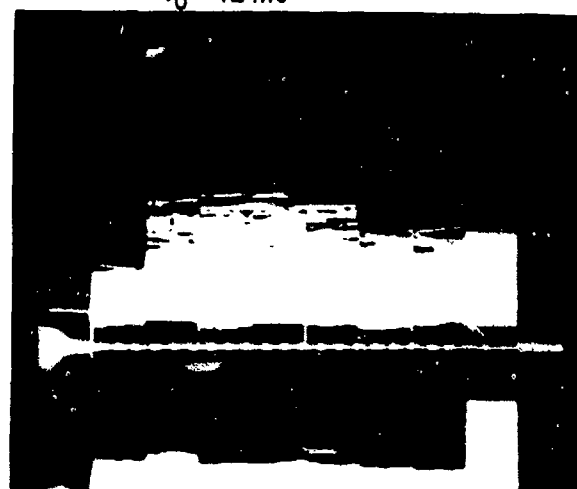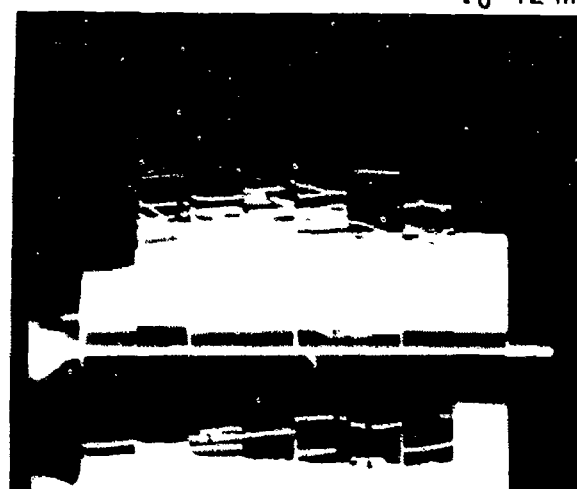
Fig. 39 (Continued)

(1-s INTEGRATION)

$\tau_0 = 12$ ms

$\tau_0 = 18$ ms

$\tau_0 = 12$ ms

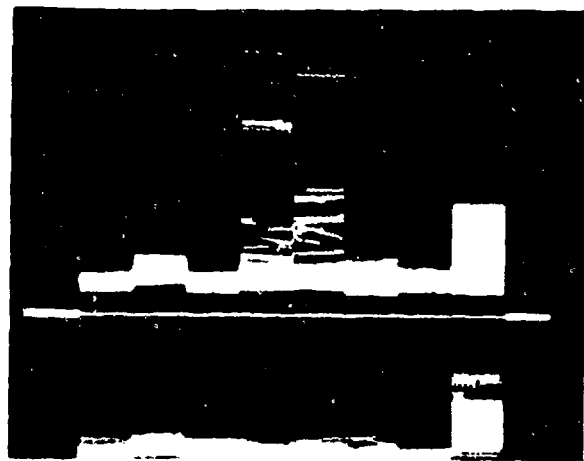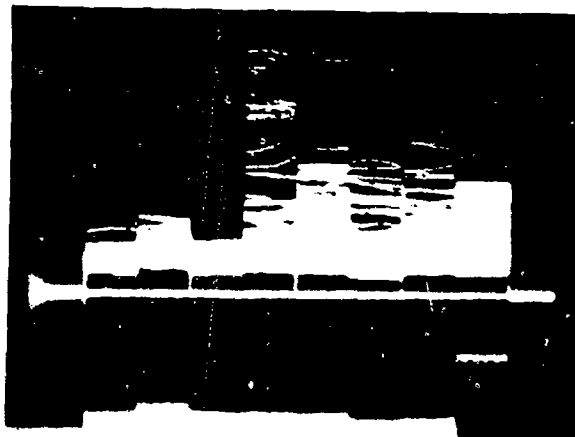$\tau_0 = 8$ ms

$\tau_0 = 4$ ms

(5-s INTEGRATION)

Fig. 40(a) — Performance of 2-delay sea-scatter rejection circuit for several different delay settings (5-Hz modulated target signal in range gate 8). Photos are for 5-s integration time except for top photo, which has 1-s integration time. Top trace in each unprocessed, bottom trace processed, for sea state 4 and vertical polarization
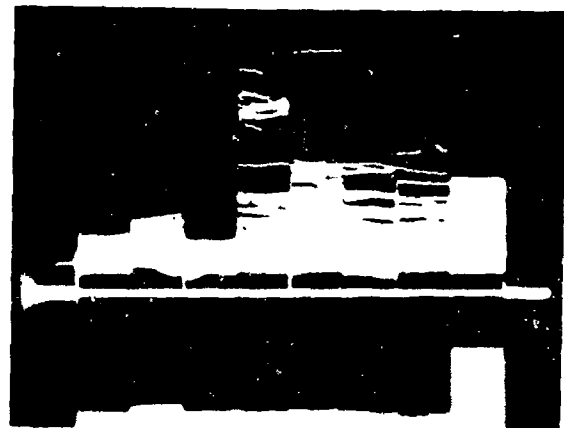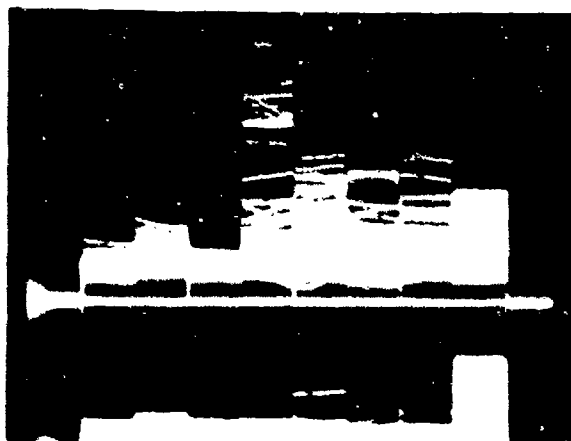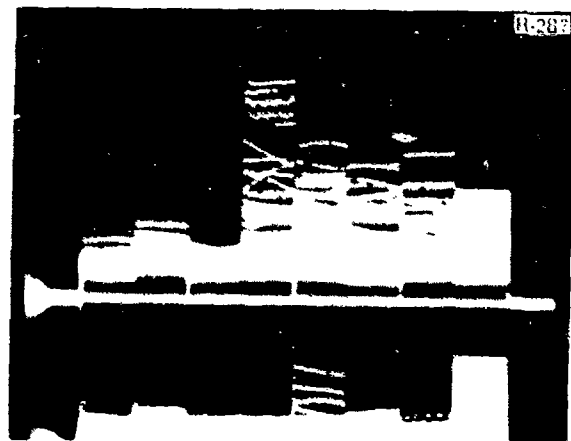
(1-s INTEGRATION)

$\tau_0 = 12$ ms

$\tau_0 = 18$ ms

$\tau_0 = 12$ ms

$\tau_0 = 8$ ms

(5-s INTEGRATION)

$\tau_0 = 4$ ms

Fig. 40(b) — Performance as in Fig. 40(a), here for sea state 4 and horizontal polarization

(1-s INTEGRATION)

$\tau_0 = 12$ ms

$\tau_0 = 18$ ms

$\tau_0 = 12$ ms

$\tau_0 = 8$ ms

$\tau_0 = 4$ ms

(5s-INTEGRATION)

Fig 40(c) — Performance as in Fig 46(a), here for sea state 2 and vertical polarization

(1-s INTEGRATION)

$\tau_0 = 12$ ms

$\tau_0 = 18$ ms
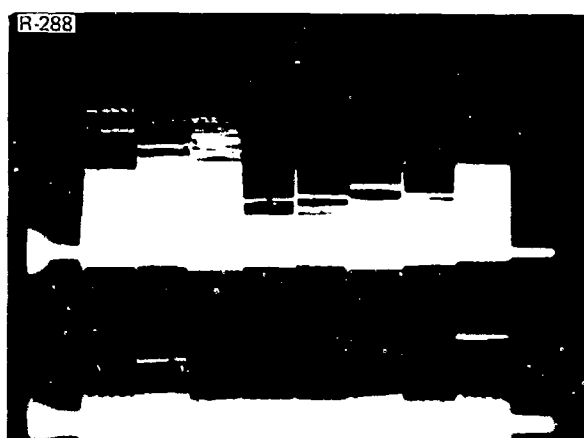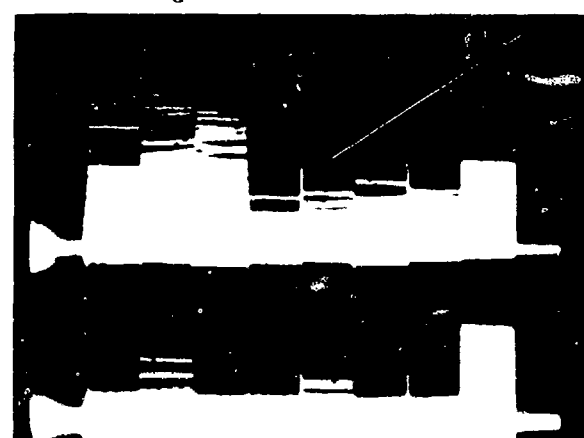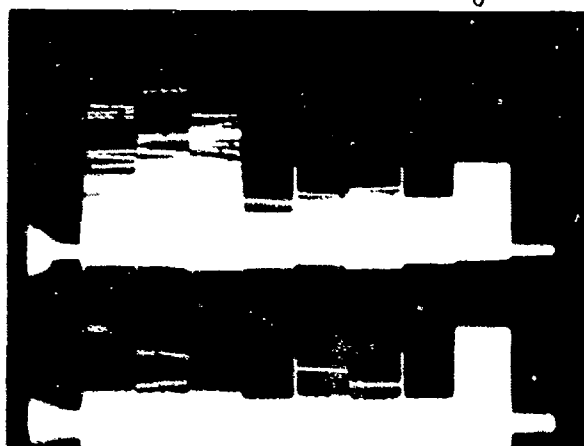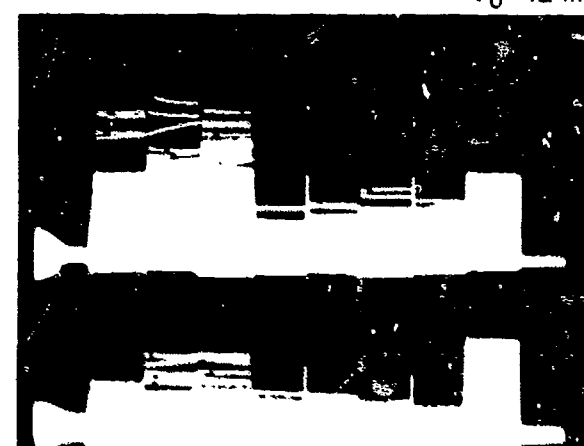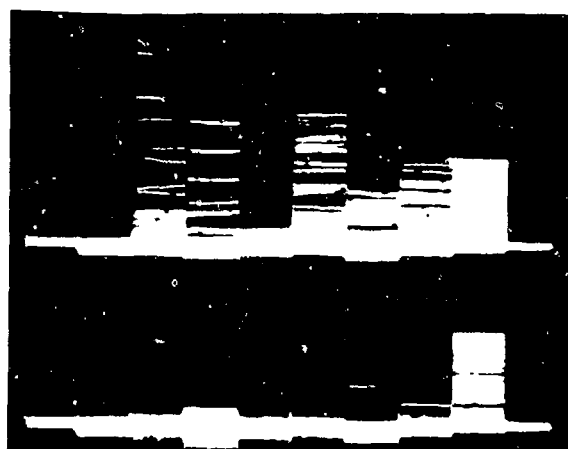
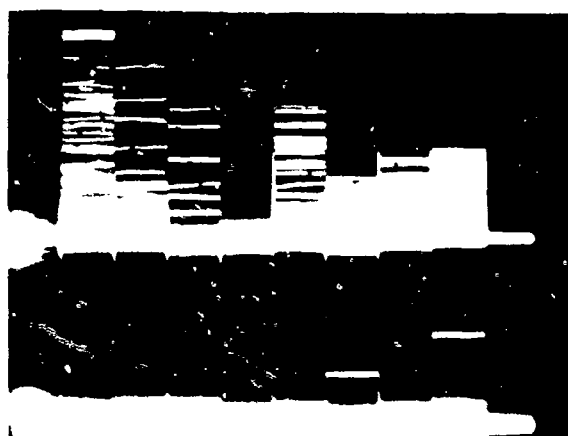$\tau_0 = 12$ ms

$\tau_0 = 8$ ms

$\tau_0 = 4$ ms

(5 s- INTEGRATION)

Fig. 40(d) — Performance as in Fig. 40(a), here for sea state 2 and horizontal polarization
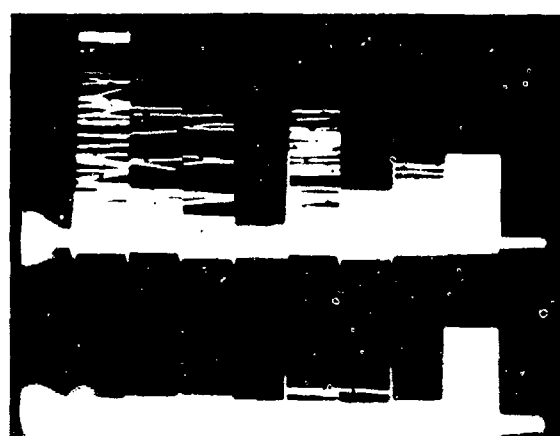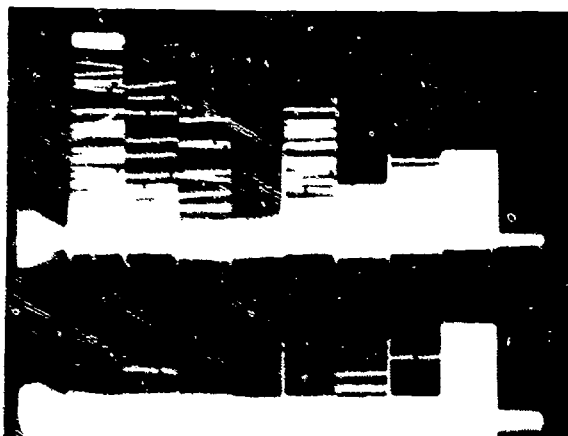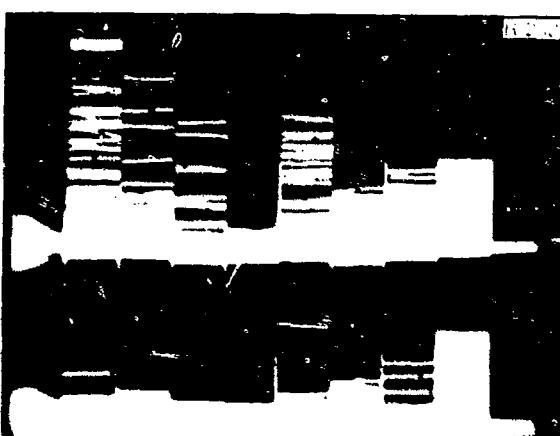
Table 2 — Performance of a Five-Delay Sea Scatter Discriminant for Various Delay Times

Data Parameters	Delay Increment (ms)	Sea-Scatter Detections 0.6 m² Det. Level (% time)						5-Hz Target Retention (% visible time)
		CH 1	CH 2	CH 3	CH 4	CH 5	CH 6	
Vert. Pol.	0	10.7	14.6	11.4	15.8	13.4	8.8	100
Sea State 5	4	0.26	0.72	0.18	0.46	0.36	0.14	99.666
0° obs. angle	(20 total)							
3° inc. angle	12	0.005	0.01	0.005	0.015	0.01	0.000	99.625
	(60 total)							
	20	0.015	0.03	0.000	0.015	0.005	0.000	98.864
	(100 total)							
Hor. Pol.	0	4.1	4.9	4.0	6.7	7.9*	6.3*	100
Sea State 5	4	0.11	0.22	0.08	0.31	0.49	0.29	99.796
0° obs. angle	(20 total)							
3° inc. angle	12	0.005	0.01	0.005	0.03	0.39	0.12	99.320
	(60 total)							
	20	0.000	0.02	0.000	0.025	0.20	0.05	98.845
	(100 total)							

*Data partially saturated on CHs 5 and 6.

When examined on an amplitude-density basis, the distributions of scatter for vertical polarization tend to be more exponential (linear slope on Rayleigh statistical coordinates) while the distributions for horizontal polarization exhibit a bow or inflection in the low-level portion which becomes more apparent at lower sea states. This inflection is believed to be one result (or indicator) of the sporadic burst character of the scatter observed with horizontal polarization.

5. Multipath effects occur which appear to involve the disturbed sea (whitecaps) and its image on the tilted wave surface.

6. High-resolution-radar return from floating rigid objects generally exhibits lower amplitude-modulation frequencies than does sea return. Amplitude distributions, on the other hand, may be quite similar.

7. A multiple-delay rejection circuit can detect and block most high-frequency-modulated sea-return signals and pass lower-frequency-modulated target-return signals.

CONCLUSIONS

The experimental measurement program has determined that one dominant characteristic of low-incidence-angle, high-resolution radar sea scatter is a relatively rapid and high-percentage pulse-to-pulse amplitude modulation. The high-resolution sea scatter has also been found to be nonuniform in time with quiet periods of relatively low level returns interspersed with high-level, targetlike spikes. High-level returns for both horizontal and vertical radar polarizations have been observed with the formation of turbulent breaking water (as indicated by the visual observation of whitecaps). Lower level returns for vertical radar polarization have been associated with the small-wave or ripple structure, while a distinctive burstlike scatter for horizontal radar polarization has been associated with preferentially aligned sharp wave crests.

The measured differences in the modulation characteristic of a disturbed sea surface and of rigid floating targets suggests that a discriminant based on percentage modulation vs time could be used to reject sea scatter. Tests with recorded sea-scatter data have shown that this type of discriminant will block typical sea-scatter signals and pass a target signal. Specifically, a five-delay rejection circuit with internal delays of 12 ms and a total delay of 60 ms effectively rejected X-band sea-scatter spikes and passed simulated target signals which were sawtooth modulated at 5 Hz.

A subject radar using this type of processing would be required to dwell on or revisit the same region over a sufficiently long time period (60 ms) to detect and suppress the sea return. Within these restrictions, a radar processor could employ the amplitude-modulation discriminant and markedly reduce the probability of sea-scatter false alarms yet still maintain detection of rigid targets.

Although the high-resolution measurements cited in this report were somewhat limited in scope, the observed variability with radar resolution, polarization, and observation direction suggests that much more intensive scatter research is required if a realistic radar sea-scatter model is to be formulated. It is felt that the amplitude-modulation discriminant has shown promise but that a complete evaluation of this and other discrimination techniques will also be dependent on further measurements. Specific areas of interest include the effects of still higher resolution and frequency, the impact of wave shadowing on the detection of small floating targets, and the modulation characteristic of complex-shaped rigid targets.

REFERENCES

1. B.L. Lewis and I.D. Olin, "Some Recent Observations of Sea Spikes," *IEE Conference Publication No. 144*, p. 115, 1975.

2. B.L. Lewis, J.P. Hansen, I.D. Olin, and V. Cavaleri, "High-Resolution Radar Scattering Characteristics of a Disturbed Sea Surface and Floating Debris," NRL Report 8131, July 29, 1977.

3. B.L. Lewis and I.D. Olin, "Experimental Study and Theoretical Model of High-Resolution Radar Backscatter from the Sea," Radio Science 15 (4), 815-828 (July-Aug. 1980).

4. H. Sittrop, "Radar Reflection Characteristics of Sea Clutter," presented at AGARD Conference on New Devices, 1976.

5. M.W. Long, *Radar Reflectivity of Land and Sea*, D. C. Heath and Co., Lexington, Mass., 1975, Chapter 6.

6. G. Bishop and E.H. Boyenval, "Amplitude Distribution Characteristics of X-Band Radar Sea Clutter and Small Surface Targets," Memo No. 2348, Royal Radar Establishment, Fort Halstead, Sevenoaks, Kent, Great Britain, 1978.

7. M.W. Long, *Radar Reflectivity of Land and Sea*, D. C. Heath and Co., Lexington, Mass., 1975, Chapter 5, p. 180.

8. A.I. Kalmykov, A.S. Kurekin, Yu.A. Lamenta, I.Ye. Ostrovskiy, and V.V. Pustovoytenko, "Scattering of Microwave Radiation by Breaking Sea Waves," translated from Gor'kiy Radiofizika 19 (9), 1315-1321 (1976).

9. A.I. Kalmykov and V.V. Pustovoyten ., "On Polarization Features of Radio Signals Scattered from the Sea Surface at Small Grazing Angles," J. Geophys. Res. 81, 1960-1964 (1976).

10. M.W. Long, "On a Two Scatterer Theory of Sea Echo," IEEE Trans. Antennas Propag. AP-22 (5), 667-672, (Sept. 1974).